Antimony distribution and mobility in different types of waste derived from the exploitation of stibnite ore deposits

E. Álvarez-Ayuso [a,*], A. Murciego [b], M.A. Rodríguez [c], L. Fernández-Pozo [c], J. Cabezas [c], J.M. Naranjo-Gómez [d], R. Mosser-Ruck [e]

[a] Department of Environmental Geochemistry, IRNASA (CSIC), C/ Cordel de Merinas 40-52, 37008 Salamanca, Spain
[b] Department of Geology, Salamanca University, Plza. de los Caídos s/n, 37008 Salamanca, Spain
[c] Department of Environmental Resources Analysis, Extremadura University, Avda. Elvas s/n, 06071 Badajoz, Spain
[d] Agricultural School, Extremadura University, Avda. de Adolfo Suárez s/n, 06007 Badajoz, Spain
[e] Georessources UMR 7359 CNRS-UL, Université de Lorraine, BP 70239, Vandœuvre-lès-Nancy 54506 Cedex, France

HIGHLIGHTS

- Characterization of Sb mine waste rocks (MWR)/mine tailings (MT)/smelting waste (SW)
- Main Sb-bearing phases: natrojarosite, Fe or/and Fe—Sb (oxyhydr)oxides, and tripuhyite
- Leachable Sb in MWR/MT makes them not acceptable at hazardous waste landfills.
- Low impact of competing anions: desorbable Sb fraction <0.01% (SW) and <0.8% (MWR/MT)
- Reducing conditions could mobilize high Sb levels from MWR/MT (4.6%/3.3% of total Sb).

GRAPHICAL ABSTRACT
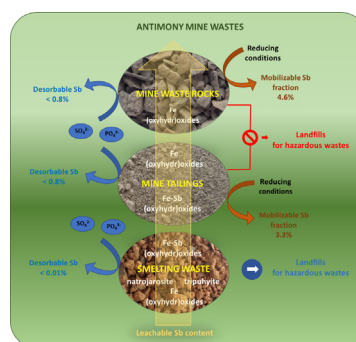
ABSTRACT

Wastes derived from the exploitation of stibnite ore deposits were studied to determine their mineralogical, chemical, and environmental characteristics and establish the Sb distribution and the current and long-term risks of Sb mobilization. Representative samples of mine waste rocks, mine tailings, and smelting waste were studied by X-ray powder diffraction, polarized light microscopy, electron microprobe analysis, and digestion, leaching, and extraction procedures. The main Sb-bearing minerals and phases identified in the smelting waste were natrojarosite, iron (oxyhydr)oxides, mixtures of iron and antimony (oxyhydr)oxides, and tripuhyite; those in the mine tailings and mine waste rocks were iron (oxyhydr)oxides and/or mixtures of iron and antimony (oxyhydr)oxides. Iron (oxyhydr)oxides and natrojarosite had high Sb contents, with maximum values of 16.51 and 9.63 wt% Sb_2O_5, respectively. All three types of waste were characterized as toxic; the mine waste rocks and mine tailings would require pretreatment to decrease their leachable Sb content before they would be acceptable at hazardous waste landfills. Relatively little of the Sb was in desorbable forms, which accounted for <0.01 and <0.8% of the total Sb content in the smelting waste and mine waste rocks/mine tailings, respectively. Under reducing conditions, further Sb mobilization from mine waste rocks and mine tailings could occur (up to 4.6 and 3.3% of the total content, respectively), considerably increasing the risk that Sb will be introduced into the surroundings. Although the smelting waste had the highest total Sb content, it showed

* Corresponding author.
  E-mail address: esther.alvarez@irnasa.csic.es (E. Álvarez-Ayuso).

the lowest risk of Sb release under different environmental conditions. The significant Fe levels in the smelting waste facilitated the formation of various Fe compounds that greatly decreased the Sb mobilization from these wastes.

1. Introduction

Antimony is a trace element that is 62nd in abundance in Earth's crust (Wedepohl, 1995), with typical contents ranging from 0.1 to 0.9 mg kg^{-1} (Kabata-Pendias and Mukherjee, 2007). It can occur in four oxidation states ($-$III, 0, III, and V) and is most commonly found in either the trivalent or pentavalent oxidation state in geochemical samples (Filella et al., 2002). It exhibits chalcophilic behavior (Filella et al., 2002; Kabata-Pendias and Mukherjee, 2007; Reimann et al., 2010; Johnston et al., 2020), and thus combines readily with sulfur to form either single or mixed sulfides, mainly with copper, lead, and silver (Anderson, 2001; Filella et al., 2002). Although more than 100 Sb minerals occur in nature (Anderson, 2001; Reimann et al., 2010; Qin et al., 2017), only a few of them are economically exploitable ores (Qin et al., 2017), and stibnite (Sb_2S_3) is the primary profitable source of Sb (Anderson, 2001).

The use of Sb and its compounds has increased in recent decades; they are currently used in a wide variety of products and industrial processes (Oorts et al., 2008; Dupont et al., 2016). Antimony is most commonly used as a flame retardant in plastics, textiles, adhesives, coatings, and electronics (approximately 50%) (Dupont et al., 2016; Hockmann et al., 2020) or as a hardening agent in lead alloys for the manufacture of batteries (approximately 35%) and ammunition (Dupont et al., 2016; Hockmann et al., 2020). Other important applications include catalysts for the production of polyethylene terephthalate, decolorizing agents in glass, pigments in paints, and ceramic opacifiers (Filella et al., 2002; Oorts et al., 2008; Ackermann et al., 2009; Dupont et al., 2016; Multani et al., 2016; Herath et al., 2017). Additionally, in recent years Sb has found increasing applications in high-tech fields (Zhang et al., 2020), for example, in the semiconductor industry for the manufacture of Hall sensors, infrared detectors, and diodes; for the production of low-power electronic devices; and for the fabrication of new thermoelectric modules for power generation or cooling (Yeh et al., 2013; Multani et al., 2016; Qin et al., 2017; Vinayakumar et al., 2018; Zhang et al., 2020).

The continuous increase in the exploitation of Sb resources to satisfy growing demand has resulted in a concomitant release of Sb to the environment. Thus, the exploitation of Sb ore deposits is regarded as the primary anthropogenic emission source of this element (Guo et al., 2014; Herath et al., 2017) and has serious negative impacts on the ecosystems of affected areas. Very high Sb concentrations have been found in the soils and water bodies of mining-impacted areas [more than 10,000 mg kg^{-1} (Baroni et al., 2000; Okkenhaug et al., 2011; Qi et al., 2011) and 5 mg L^{-1} (Cidu et al., 2014), respectively]. Antimony has no known biological function and is toxic for the majority of organisms above certain threshold values (Alloway, 1995; McBride, 1994; Filella et al., 2007). Culturable soil bacteria and fungi can be significantly inhibited by Sb (He et al., 2019). Plants can readily take up Sb if it is present in soluble forms (Baroni et al., 2000; Kabata-Pendias and Mukherjee, 2007). Antimony can have various toxic effects on Sb-intolerant plants, for example, growth retardation, alterations in root system morphology and development, the inhibition of photosynthesis, limited uptake and disturbed distribution of some essential elements, and decreased synthesis of some metabolites (Feng et al., 2013, 2016). By contrast, tolerant plants can accumulate high Sb levels in their edible parts (Feng et al., 2013) and thus pose an important risk of human exposure to Sb; estimated daily intake values indicate that they represent an important percentage of the tolerable daily intake (360 µg of Sb) (Biddau and Cidu, 2017) or even exceed it (Wu et al., 2011). Thus, the consumption of

cereals (rice and corn, mainly the former) and vegetables has been identified as the dominant route of Sb entry into the body via dietary exposure for residents of mining areas, accounting for close to 62% (Wu et al., 2011). In addition to oral intake, Sb exposure can also occur by inhalation and dermal contact (Saerens et al., 2019), although the latter is considered to be an unimportant systemic route (Boreiko and Rossman, 2020). In humans, long-term intoxication can have various adverse effects, including respiratory diseases (e.g., rhinitis, chronic cough, bronchitis, pleural adhesions, emphysema, and pneumoconiosis), reproductive changes, immune system disorders, gastrointestinal problems, cardiovascular system complications, and possibly lung cancer (Cooper and Harrison, 2009; Sundar and Chakravarty, 2010; Li et al., 2018; Saerens et al., 2019). Because of its negative impacts on human and environmental health, there is increasing interest in the processes responsible for the release and attenuation of Sb in mining regions.

Stibnite readily dissolves under oxidizing conditions (Vink, 1996; Ashley et al., 2003). Its dissolution rate is increased by abiotic factors such as mild basic conditions (Biver and Shotyk, 2012; Li et al., 2019), light irradiation (Hu et al., 2015), and the presence of pyrite (FeS_2) (Beauchemin et al., 2012; Flakova et al., 2012; Yan et al., 2020). In addition, dissolution can be biotically mediated (Loni et al., 2020). Stibnite weathering products can reduce the release of Sb to the environment. In the first stages of stibnite weathering, oxides are formed, along with soluble antimonates and/or antimony sulfates (Filella et al., 2009; Majzlan et al., 2016). Common oxides are senarmontite (α-Sb_2O_3), valentinite (β-Sb_2O_3), cervantite (α-Sb_2O_4), and stibiconite [$Sb_3O_6(OH)$]; stibiconite is most frequently reported in mining areas (Roper et al., 2012). Under oxidizing conditions, stibiconite is stable within a wide pH range (approximately 2–10), with a solubility of hundreds of µg Sb L^{-1}; the lowest values occur at a pH of approximately 7.5 (Biver and Shotyk, 2013). The solubility of stibiconite is much lower than those reported for other oxides (Filella et al., 2009; Biver and Shotyk, 2013). As weathering progresses, other secondary Sb phases appear, including minerals of the roméite group ($Ca_2Sb_2O_7$) (Courtin-Nomade et al., 2012; Lalinská-Voleková et al., 2012; Dordević et al., 2019; Jurkovic et al., 2019a) and iron antimonates, where tripuhyite ($FeSbO_4$) is the most commonly found (Majzlan et al., 2011; Courtin-Nomade et al., 2012; Lalinská-Voleková et al., 2012; Jurkovič et al., 2019b; Borčinová Radková et al., 2020). These minerals are highly insoluble (Diemar et al., 2009; Selim, 2012; Multani et al., 2016), particularly tripuhyite, which has a solubility of <10 µg Sb L^{-1} (Selim, 2012; Multani et al., 2016). Moreover, it can also occur within a wide pH range (Multani et al., 2016). However, its kinetics of formation is considered to be quite slow (Majzlan et al., 2016).

In addition to studies on the formation, dissolution, and transformation of Sb minerals, research has assessed the potential risks posed by different types of waste derived from the exploitation of stibnite deposits (Guo et al., 2014; Flaková et al., 2017; Ren et al., 2018; Zhang et al., 2019; Zhou and Hursthouse, 2019; Zhou et al., 2020; Cappuyns et al., 2021). Most of these studies have focused on determining the total Sb content (Zhou and Hursthouse, 2019; Zhou et al., 2020; Cappuyns et al., 2021) or Sb leachability of wastes using either static or dynamic leaching tests (Ren et al., 2018; Zhang et al., 2019; Zhou and Hursthouse, 2019; Cappuyns et al., 2021). These studies have shown that although the total Sb content varies within a wide range, it typically reaches values up to approximately 15,000 mg kg^{-1}, with leachable fractions close to 1%. Antimony leachability is affected by several factors and increases with increasing temperature and decreasing grain size. Although some risk characteristics have been identified,

there is relatively little information on the distribution and mobilization of Sb in mine wastes under various environmental conditions (Guo et al., 2014; Flaková et al., 2017). Further research is crucial to establishing appropriate measures to minimize Sb migration from mine wastes and the concomitant pollution of surrounding areas.

The main aim of this study was to characterize different types of waste derived from the exploitation of stibnite ore deposits, specifically, mine waste rocks, mine tailings, and smelting waste, and to determine their mineralogical and chemical composition and environmental behavior and thus establish their Sb distribution and the current and long-term risks of Sb mobilization.

2. Materials and methods

2.1. Study area

The former San Antonio mine was considered in this study. Its location and the geological map of the area are shown in Fig. 1 (Gumiel et al., 2002). This mine exploited the main stibnite deposit in Spain from 1940 to 1986. It is located approximately 10 km southwest of the village of Alburquerque in the northwestern part of the province of Badajoz. It is a hydrothermal deposit hosted in black limestones, breccias, calcareous shales, and some siliceous rocks, where the main mineral association is quartz + stibnite + scheelite ($CaWO_4$); however, berthierite ($FeSb_2S_4$) and pyrite are also present, with arsenopyrite (FeAsS) and antimony as accessory minerals (Gumiel and Arribas, 1987). The exploitation of this stibnite ore deposit, including mining, ore processing, and metallurgical activities, generated large volumes of waste. Mine waste rocks were accumulated in dumps, whereas mine tailings and smelting waste were deposited separately on the land. Significant amounts of waste remain

in the mining area. The volume of mine waste has been estimated to be approximately 3 t (Murciego et al., 2007).

2.2. Sampling

Mine waste rocks, mine tailings, and smelting waste were sampled. Mine waste rocks were collected from a small mine dump characteristic of this mining area. Small rocks (<10 mm) are accumulated in this type of dump. Weathering profiles were not observable in the dump. Mine waste rocks were sampled from the surface of the mine dump (0–20 cm) at different places, mixed, and homogenized to generate a composite sample. Mine tailings and smelting waste were collected at random sites on the surface (0–20 cm) of their deposition locations, mixed, and homogenized to generate a composite sample of each type of waste. The sampled mine waste rocks, mine tailings, and smelting waste were subjected to mineralogical, chemical, and environmental characterization.

Additionally, to assess the contamination of aquatic systems in the area affected by this waste, water samples were collected in the mining area from streams [small creeks (C1 and C2), tributaries of the Gévora river (R1a and R1b)], ponds (P1, P2, and P3), and wells (W1). Fig. 1 shows the locations of the water sampling points. The collected water samples were filtered through 0.45 μm membrane filters in high-density polyethylene bottles. Upon filtration, one aliquot was acidified with ultrapure HNO_3 for element analysis and the other was used for alkalinity determination.

2.3. Characterization of mine waste rocks, mine tailings, and smelting waste

2.3.1. Mineralogical characterization

The mineralogical characterization was performed using powder X-ray diffraction (XRD) and polarized light microscopy. XRD analyses of
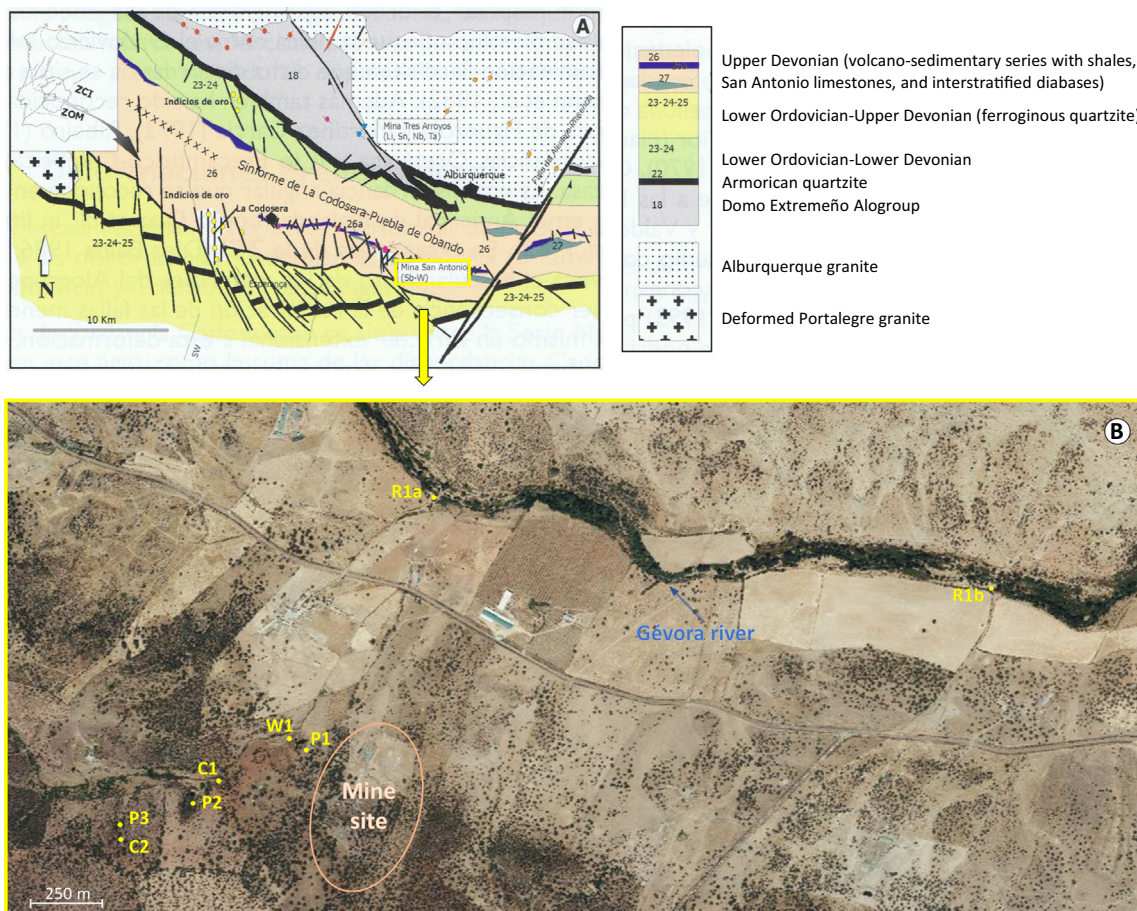

Fig. 1. Location of San Antonio mine and geological map of the area (A) and location of water sampling points (B).

unoriented powder samples were conducted using a D8 Advance diffractometer (Bruker) with Cu Kα radiation. Rietveld refinement of the XRD patterns was performed for quantitative mineralogical analysis. Polished thin sections of waste samples embedded in resin were examined by polarized light microscopy using a Nikon Eclipse E400 POL optical microscope operating in transmitted and reflected light.

2.3.2. Chemical characterization

The pseudo-total contents of Sb and other major and minor/trace elements (Al, As, Ca, Fe, K, Mg, Mn, Na, P, and S) were determined in triplicate by aqua regia digestion of finely ground waste samples at 190 °C for 15 min using a Milestone Ethos Plus microwave oven. Following digestion, the extracts were analyzed by inductively coupled plasma-atomic emission spectrometry (ICP-AES) using a Varian 720-ES spectrometer. The accuracy of the method was assessed using standard reference materials (NIST SRM 2709a and NIST SRM 2711a); the recoveries were within 90–110%.

Spot chemical analyses and backscattered electron (BSE) images of possible Sb-hosting phases were performed using electron microprobe analysis (EMPA). Carbon-coated polished thin sections of waste samples embedded in resin were analyzed in wavelength-dispersive mode using a JEOL Superprobe JXA-8900M electron probe microanalyzer at CNME. The following elements were analyzed: Sb, S, Fe, Ca, K, Na, Si, Al, and As, and the following minerals were used as calibration standards: native Sb for Sb, galena for S, almandine for Fe, kaersutite for Ca, microcline for K, albite for Na and Si, sillimanite for Al, and gallium arsenide for As.

2.3.3. Environmental characterization

The following properties were determined in the environmental characterization: pH, electrical conductivity (EC), net neutralization potential (NNP), toxicity, leaching behavior, effect of competing anions, and chemical fractionation. All parameters were determined in triplicate.

The pH of crushed samples (<0.250 mm) of the mine waste was determined potentiometrically using the water-saturated paste method, and the EC was measured conductometrically by the same method.

The NNP of the mine waste was estimated as the difference between its neutralization potential (NP) and acid potential (AP) expressed in kg CaCO$_3$ t^{-1}. The NP was assessed according to the method of Sobek et al. (1978). Crushed mine waste samples (<0.250 mm) treated with 0.1 M or 0.5 M HCl were heated under stirring to nearly boiling. After the samples were neutralized, the cooled solutions were titrated with 0.1 M or 0.5 M NaOH to determine the acid consumed by the mine waste samples. The AP was obtained directly from the sulfur content of the mine waste according to the following equation: AP = 31.25 wt% S, which expresses the maximum theoretical quantity of acid that could be produced from the waste. The sulfur content of the waste was assessed as the difference between the pseudo-total S content and the S content present as sulfate, as determined by acid digestion with aqua regia and concentrated HCl, respectively.

The toxicity of the mine waste was determined according to the toxicity characteristic leaching procedure (TCLP). Mine waste samples (<9.5 mm) were shaken for 18 h with buffered acetic acid solutions (pH 4.93 ± 0.05) at a liquid/solid (L/S) ratio of 20 L kg^{-1} using a rotary shaker at 30 rpm. Following sedimentation and filtration, the extracts were analyzed for Sb and As using ICP-AES.

The leaching behavior of the mine waste was determined according to the European leaching test EN-12457-4 (2002). Mine waste samples (<10 mm) were shaken with deionized water at an L/S ratio of 10 L kg^{-1} for 24 h using a rotary shaker at 10 rpm. Following sedimentation and filtration, the extracts were analyzed for Sb, As, and S using ICP-AES.

The effect of competing anions on the desorption of Sb and As from the mine waste was assessed by consecutive extractions with 0.05 M (NH$_4$)$_2$SO$_4$ (shaking period: 4 h) and 0.05 M NH$_4$H$_2$PO$_4$ (shaking period: 16 h) using an L/S ratio of 25 L kg^{-1}, as described by Wenzel et al. (2001). These extractions were performed to identify non-specifically and specifically adsorbed metalloids, respectively.

The chemical fractionation of Sb and As in the mine waste was determined according to the modified "Bureau Communautaire de Référence" (BCR) sequential extraction protocol established by Rauret et al. (1999). This procedure is recognized as a valuable tool for assessing the element mobility from different environmental samples in various complex scenarios (Pueyo et al., 2003, 2008) and has been applied successfully to mine wastes (Álvarez-Valero et al., 2009; Courtin-Nomade et al., 2016). It consists of four steps that target the weak acid-soluble fraction, reducible fraction, oxidizable fraction, and residual fraction.

2.4. Analysis of water samples

The concentrations of Sb, As, Fe, Ca, Mg, Mn, Na, K, and S were determined in collected water samples. The analysis of Fe, Ca, Mg, K, and S was performed by ICP-AES. The analysis of Sb and As was performed by inductively coupled plasma mass spectrometry (ICP-MS). An Agilent 7900 ICP-MS instrument was employed for these analyses. The analysis accuracy was estimated using standard reference materials (NIST SRM 1643f trace elements in water and SPEX Certiprep PLS9-3X S solution). The estimated errors were <5%. The analysis precision was better than 5% as determined by three replicate determinations. Alkalinity (Alk) was determined by titration with 0.02 M H$_2$SO$_4$ to a pH of 4.5. The pH and EC of water samples were measured on site using a HANNA Instruments HI9811-5 portable analyzer.

3. Results and discussion
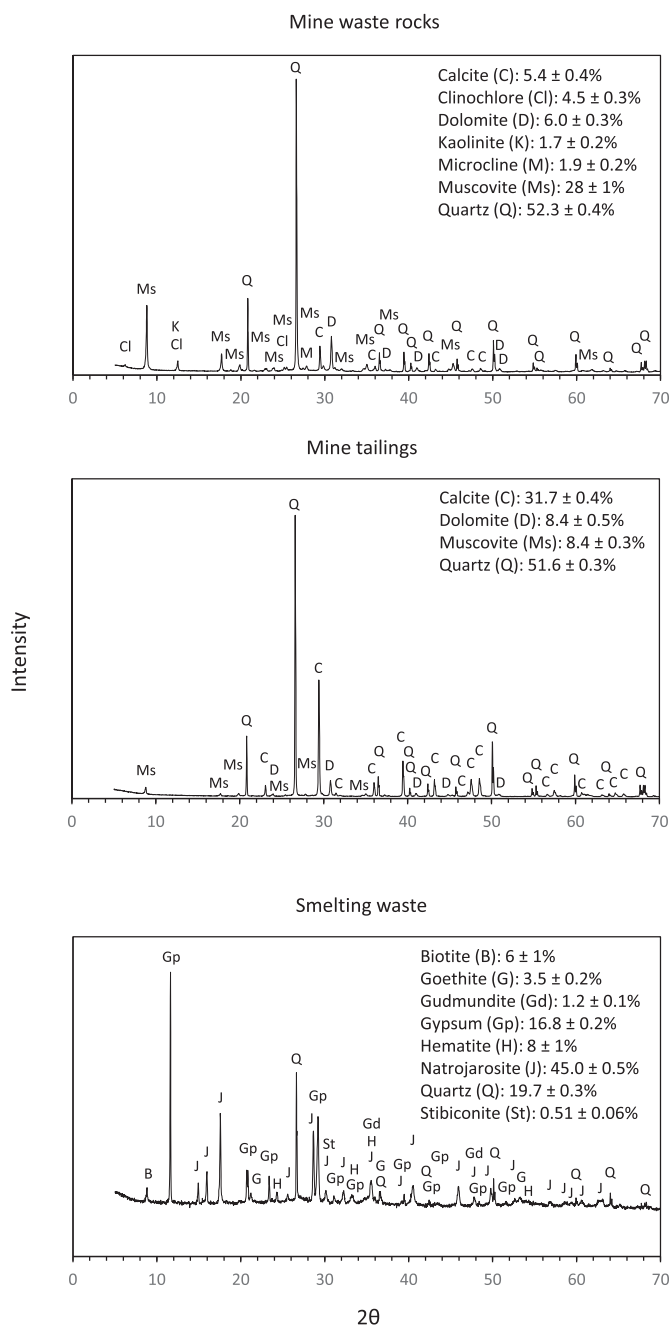
3.1. Mineralogical characterization

Fig. 2 shows the mineralogical composition of the mine waste as determined by XRD. The mine waste rocks and mine tailings were composed primarily of carbonate minerals (approximately 11 and 40%, respectively) and silicate minerals (approximately 89 and 60%, respectively), and carbonates were much more abundant in the mine tailings. The smelting waste had a more heterogeneous composition of silicate minerals, iron (oxyhydr)oxides [goethite (α-FeOOH) and hematite (α-Fe$_2$O$_3$)], sulfates [gypsum (CaSO$_4$·2H$_2$O)], iron hydroxy sulfates [natrojarosite (NaFe$_3$(SO$_4$)$_2$(OH)$_6$)], and Sb minerals [stibiconite and gudmundite (FeSbS)]. Natrojarosite was most abundant (45%), followed by silicate minerals (26%), gypsum (17%), and iron (oxyhydr)oxides (11%), whereas the Sb mineral content was relatively low (<2%).

Microscope and BSE images of the mine wastes are shown in Fig. 3. Polarized light microscopy analyses confirmed the presence of most of the minerals detected by XRD. Additionally, other phases were also identified in each type of mine waste.

In the mine waste rocks, in addition to carbonates and silicate minerals, iron (oxyhydr)oxides were also present, with small amounts of pyrite, arsenopyrite, and cracked orange-red phases. These phases likely correspond to Fe arsenates (anisotropy was not observed); they contained relicts of arsenopyrite. Most of the iron (oxyhydr)oxides were blackish, with an opaque or almost opaque appearance; anisotropy was rarely observed. Iron (oxyhydr)oxides frequently formed fine coatings on phyllosilicates and carbonates. Reflected light observations revealed the occurrence of iron (oxyhydr)oxides as weathering products of pyrite, replacing pyrite on its crystal borders or completely replacing and pseudo-morphing pyrite crystals. The reflectance (R) of the iron (oxyhydr)oxides varied from zero to low values (R < 25%), and they exhibited few reddish internal reflections.

In the mine tailings, in addition to carbonates and silicate minerals, iron (oxyhydr)oxides, reddish-black phases, and relicts of pyrite were also observed. The iron (oxyhydr)oxides were blackish and had an opaque appearance; anisotropy was rarely observed. The iron (oxyhydr)

Mine waste rocks

Calcite (C): 5.4 ± 0.4%
Clinochlore (Cl): 4.5 ± 0.3%
Dolomite (D): 6.0 ± 0.3%
Kaolinite (K): 1.7 ± 0.2%
Microcline (M): 1.9 ± 0.2%
Muscovite (Ms): 28 ± 1%
Quartz (Q): 52.3 ± 0.4%

Mine tailings

Calcite (C): 31.7 ± 0.4%
Dolomite (D): 8.4 ± 0.5%
Muscovite (Ms): 8.4 ± 0.3%
Quartz (Q): 51.6 ± 0.3%

Smelting waste

Biotite (B): 6 ± 1%
Goethite (G): 3.5 ± 0.2%
Gudmundite (Gd): 1.2 ± 0.1%
Gypsum (Gp): 16.8 ± 0.2%
Hematite (H): 8 ± 1%
Natrojarosite (J): 45.0 ± 0.5%
Quartz (Q): 19.7 ± 0.3%
Stibiconite (St): 0.51 ± 0.06%

2θ

Fig. 2. XRD patterns and mineralogical composition of mine wastes (values are expressed together with their corresponding uncertainties).

oxides sometimes formed fine coatings on carbonates. The reflectance of the iron (oxyhydr)oxides was low (R < 25%). The reddish-black phases appeared either isolated or with iron (oxyhydr)oxides; some contained relics of pyrite. The reddish-black phases had no reflectance, with reddish internal reflections. These phases may correspond to mixtures of iron and antimony (oxyhydr)oxides, as suggested by further spot chemical analysis. Furthermore, BSE images of these phases showed different gray shades, suggesting that they are chemically heterogeneous and contain elements of different atomic numbers [lower (Fe) and higher (Sb)], as lighter elements appear darker, and heavier elements appear brighter. The possible deposition of antimony (oxyhydr)oxides with iron (oxyhydr)oxides in other mining areas has been suggested (Craw et al., 2004).

In the smelting waste, jarosite-group minerals, iron (oxyhydr)oxides, gypsum, silicate minerals, reddish-black phases, and blackish-reddish-brown phases were observed. Jarosite-group minerals and

iron (oxyhydr)oxides were very abundant. The jarosite-group minerals were yellowish-brownish-red and anisotropic, with a cracked appearance. The jarosite-group minerals sometimes appeared with iron (oxyhydr)oxides and reddish-black phases. The iron (oxyhydr)oxides were blackish and had an opaque appearance; anisotropy was rarely observed. The reflectance of iron (oxyhydr)oxides varied from very low (R < 10%) to low (R: 15–25%); those with higher reflectance may correspond to hematite. The reddish-black phases also had an opaque appearance and occurred either in isolation or with jarosite-group minerals. The reddish-black phases had no or very low reflectance (R < 10%). As indicated above, the reddish-black phases may be composed of mixtures of iron and antimony (oxyhydr)oxides. The blackish-reddish-brown phases were lighter in color (reddish-orange) at their borders, likely because of reduced grain thickness. The texture of the blackish-reddish-brown phases varied from xenomorphic to subidiomorphic and appeared to be isotropic. The reflectance of the blackish-reddish-brown phases varied from zero to very low (R < 10%), and they exhibited yellow-reddish internal reflections. These phases may correspond to tripuhyite, as suggested by further spot chemical analysis. Tripuhyite resembles iron (oxyhydr)oxides (Leverett et al., 2012; Kossoff et al., 2015), particularly in color (orange-red) (Kossoff et al., 2015) and structure (nanocrystalline with high structural disorder) (Majzlan et al., 2011; Mitsunobu et al., 2011). Consequently, tripuhyite is often misidentified as iron (oxyhydr)oxides (Leverett et al., 2012; Kossoff et al., 2015).

Stibnite was absent in the mine waste, whereas some arsenopyrite and pyrite remained. Stibnite oxidizes rapidly, within days or weeks, under atmospheric conditions (Ashley et al., 2003). It can also be dissolved under reducing conditions if alkaline conditions are present (Vink, 1996). The oxidation of stibnite proceeds more rapidly than that of arsenopyrite, which in turn oxidizes more rapidly than pyrite (Komnitsas et al., 1995; Flakova et al., 2012). Moreover, because of galvanic effects, pyrite can enhance the dissolution of stibnite and arsenopyrite when these minerals coexist (Beauchemin et al., 2012; Flakova et al., 2012; Dos Santos et al., 2017; Yan et al., 2020). Further oxidation of the remaining arsenopyrite and pyrite in the mine waste rocks/mine tailings can result in the release of acid and associated metalloids. However, both the mine waste rocks and mine tailings contained abundant minerals with high acid-buffering capacity. As a result of sulfide weathering, iron (oxyhydr)oxides and/or mixtures of iron and antimony (oxyhydr)oxides were the main secondary products formed in the mine tailings and mine waste rocks. Neither the soluble antimonates and/or antimony sulfates characteristic of the initial phases of stibnite weathering (Filella et al., 2009; Courtin-Nomade et al., 2012; Majzlan et al., 2016) nor the minerals of the roméite group, which are regarded as the ultimate oxidation products (Roper et al., 2012), were detected in the tailings or rocks. Antimony (oxyhydr)oxides reportedly occur as intermediate phases in the stibnite oxidation sequence (Roper et al., 2012), although the different kinetics of formation of secondary antimony products determines their occurrence and predominance (Majzlan et al., 2016). Thus, antimony (oxyhydr)oxides have been found to coexist with more- and less-soluble stibnite weathering products (Filella et al., 2009; Majzlan et al., 2016; Jurkovic et al., 2019a). In the smelting waste, antimony (oxyhydr)oxides coexisted with tripuhyite, which is also considered to be an ultimate oxidation product of stibnite. Other sulfide weathering products present in the mine tailings were iron (oxyhydr)oxides and natrojarosite. All these secondary products can act as important sinks of Sb and/or As. Particularly, tripuhyite is highly stable in oxidizing environments, even under strong acid conditions, exhibits very low solubility and can scavenge important amounts of Sb (Courtin-Nomade et al., 2012; Leverett et al., 2012; Multani et al., 2016).

3.2. Chemical characterization

The results of chemical analyses of bulk mine waste samples are shown in Table 1. According to these analyses, the Sb content of the
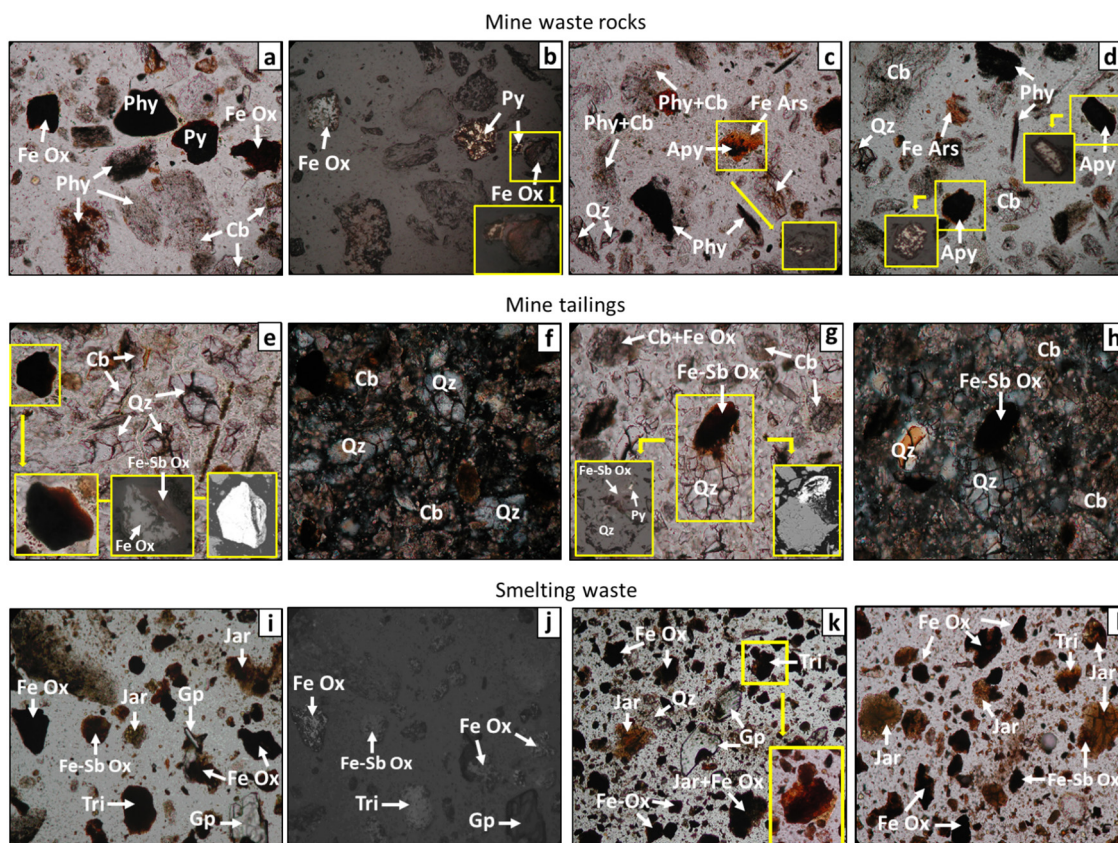
Fig. 3. Microscopy images and electron backscatter images of mine wastes.

[Notes: Microscopy images in transmitted (a, c, and d) and reflected (b) light of mine waste rocks (×200-uncrossed polars. Yellow box in b: pyrite altered to Fe (oxyhydr)oxides ×400; yellow box in c: arsenopyrite altered to Fe arsenates in reflected light; and yellow box in d: arsenopyrite in reflected light).

Microscopy images in transmitted light of mine tailings (×200-uncrossed polars (e and g) and ×200-crossed polars (f and h). Yellow box in e: Fe (oxyhydr)oxides and Fe—Sb (oxyhydr)oxides in transmitted (left) and reflected (center) light and BSE image (right) ×400. Yellow box in g: relict of pyrite in Fe—Sb (oxyhydr)oxides in reflected light (left) and BSE image (right)).

Microscopy images in transmitted (i, k, and l) and reflected (j) light of smelting waste (×200-uncrossed polars. Yellow box in k: tripuhyite ×400).

Py: pyrite, Apy: arsenopyrite, Fe Ars: Fe-arsenates, Fe Ox: Fe (oxyhydr)oxides, Cb: carbonates, Phy: phyllosilicates, Qz: quartz, Fe—Sb Ox: Fe—Sb (oxyhydr)oxides, Gp: gypsum, Tri: tripuhyite, and Jar: jarosite-group minerals].

mine waste followed the sequence smelting waste (4.72%) > mine waste rocks (0.54%) > mine tailings (0.11%). Antimony was present in the smelting waste as a major element, with contents approximately one order of magnitude higher than those in the mine waste rocks and mine tailings. Other major elements in the smelting waste were S, Na, Fe, and Ca, which is consistent with the significant natrojarosite, gypsum, and iron (oxyhydr)oxides contents. The As content of the mine waste also varied in the same sequence: smelting waste (573 mg kg^{-1}) > mine waste rocks (392 mg kg^{-1}) > mine tailings

(21.0 mg kg^{-1}), although this element was present at trace levels, which is consistent with the accessory occurrence of arsenopyrite in this deposit.

Table 2 shows the results of spot chemical analyses of possible Sb-hosting phases in each type of mine waste. In the mine waste rocks, iron (oxyhydr)oxides had the highest Sb content (up to 11.37 wt% Sb$_2$O$_5$), with an average value of 5.97 wt% Sb$_2$O$_5$. These values are consistent with those of these compounds in mine waste resulting from the exploitation of other stibnite-bearing deposits (4.0–14.6 wt% Sb$_2$O$_5$) (Craw et al., 2004; Courtin-Nomade et al., 2012; Lalinská-Voleková et al., 2012; Borčinová Radková et al., 2020). Significant amounts of As were also found (up to 11.42 wt% As$_2$O$_5$), with an average value of 3.95 wt% As$_2$O$_5$. Iron (oxyhydr)oxides can accommodate variable As amounts. Contents as high as 31.6 wt% As$_2$O$_5$ were found in iron (oxyhydr)oxides present in mine wastes (Hiller et al., 2012). Cracked orange-red phases resembling Fe arsenates had average Fe$_2$O$_3$ and As$_2$O$_5$ contents of 42.77 and 24.42 wt%, respectively; these values differ considerably from those of scorodite (ideally, 34.60 and 49.79 wt%, respectively). Their Fe/As molar ratio (2.5) is within the range (1–4) for precipitates containing poorly crystalline or amorphous Fe arsenates (AFA) (Paktunc et al., 2008), suggesting that they occur in these phases. Cracked orange-red phases had an average Sb content of 2.33 wt% Sb$_2$O$_5$, which is consistent with that of AFA in other mining areas (4.8 wt% Sb$_2$O$_5$) (Druzbicka and Craw, 2015). By contrast, scorodite can accommodate very small amounts of Sb (Kossoff et al., 2015). The Sb content of natural

Table 1
Bulk chemical analysis, pH, EC, and NNP of mine wastes.

Parameter	Mine waste rocks	Mine tailings	Smelting waste
Sb (wt%)	0.543 ± 0.007	0.113 ± 0.002	4.72 ± 0.04
As (mg kg^{-1})	392 ± 12	21.0 ± 1.8	573 ± 7
Al (wt%)	2.21 ± 0.21	0.622 ± 0.050	0.967 ± 0.060
Ca (wt%)	7.13 ± 0.02	15.2 ± 0.1	3.75 ± 0.02
Fe (wt%)	1.82 ± 0.01	0.920 ± 0.010	5.88 ± 0.07
K (wt%)	0.621 ± 0.059	0.304 ± 0.025	0.542 ± 0.016
Mg (wt%)	0.835 ± 0.010	0.647 ± 0.007	0.051 ± 0.001
Mn (wt%)	0.104 ± 0.001	0.085 ± 0.001	0.031 ± 0.001
Na (wt%)	0.155 ± 0.009	0.118 ± 0.016	1.06 ± 0.01
P (mg kg^{-1})	363 ± 10	465 ± 3	759 ± 7
S (wt%)	0.242 ± 0.002	0.040 ± 0.002	9.88 ± 0.04
pH	8.38 ± 0.10	8.64 ± 0.08	3.44 ± 0.04
EC (µS cm^{-1})	253 ± 6	117 ± 15	1270 ± 38
NNP (kg CaCO$_3$ t^{-1})	194 ± 8	446 ± 13	−41.2 ± 2

Table 2
Spot chemical analyses of Sb-bearing phases in mine wastes.

	Phases	%								
		Sb_2O_5	As_2O_5	Al_2O_3	Fe_2O_3	SO_3	K_2O	Na_2O	SiO_2	CaO
Mine waste rocks	Fe (oxyhydr)oxides (n = 5)	5.97 (1.65–11.37)	3.95 (0.02–11.42)	0.33 (0.05–1.12)	74.21 (47.48–88.40)	0.15 (0.12–0.19)	0.03 (0.01–0.05)	(n.d.–0.40)	1.34 (0.14–2.32)	2.29 (0.69–4.34)
	Phyllosilicates (n = 7)	2.15 (1.11–3.11)	(n.d.–0.02)	31.11 (24.86–36.16)	0.77 (0.63–1.03)	(n.d.–0.03)	7.46 (5.97–8.14)	0.77 (0.41–1.17)	45.02 (32.13–50.60)	0.04 (0.04–0.06)
	Fe arsenates (n = 4)	2.33 (1.49–3.19)	24.42 (21.73–27.21)	1.40 (0.38–2.44)	42.77 (40.87–44.87)	0.12 (0.11–0.12)	0.08 (0.07–0.08)	0.22 (0.13–0.28)	1.03 (0.74–1.42)	5.29 (4.69–5.78)
	Carbonates (n = 9)	0.24 (0.14–0.43)	n.d.	(n.d.–0.63)	0.69 (0.28–1.00)	(n.d.–0.08)	(n.d.–0.03)	(n.d.–0.02)	n.d.	46.82 (42.00–51.08)
	Phases	Sb	As	Al	Fe	S	K	Na	Si	Ca
	Arsenopyrite (n = 8)	0.11 (0.06–0.22)	39.68 (33.39–42.91)	(n.d.–1.18)	35.16 (33.87–36.14)	18.36 (9.62–23.05)	(n.d.–0.01)	n.d.	(n.d.–0.25)	(n.d.–0.08)
	Pyrite (n = 4)	0.07 (0.06–0.07)	(n.d.–2.23)	(n.d.–1.94)	43.23 (40.77–45.79)	46.17 (38.70–53.74)	n.d.	n.d.	(n.d.–0.11)	0.37 (0.04–0.72)
	Phases	Sb_2O_5	As_2O_5	Al_2O_3	Fe_2O_3	SO_3	K_2O	Na_2O	SiO_2	CaO
Mine tailings	Fe (oxyhydr)oxides (n = 4)	2.28 (0.85–3.73)	0.09 (0.01–0.16)	0.10 (0.07–0.12)	90.27 (89.64–90.99)	0.22 (0.14–0.27)	(n.d.–0.01)	n.d.	0.51 (0.38–0.61)	0.37 (0.35–0.38)
	Reddish-black phases (Fe–Sb (oxyhydr)oxides) (n = 5)	18.64 (14.60–21.33)	0.58 (0.49–0.74)	2.03 (1.26–2.89)	36.59 (26.97–48.90)	0.46 (0.13–1.07)	0.13 (0.11–0.14)	0.07 (0.03–0.15)	8.29 (6.27–9.94)	2.70 (1.70–3.38)
	Phyllosilicates (n = 4)	1.30 (1.19–1.44)	0.04 (0.01–0.06)	33.89 (33.87–34.01)	1.35 (0.58–2.10)	0.97 (0.04–1.92)	7.80 (7.68–7.91)	0.97 (0.85–1.11)	43.23 (42.78–43.57)	0.09 (0.07–0.10)
	Carbonates (n = 21)	0.21 (0.13–0.39)	n.d.	(n.d.–1.96)	0.62 (0.02–2.74)	(n.d.–0.12)	(n.d.–0.42)	(n.d.–0.05)	(n.d.–8.17)	48.23 (43.47–53.26)
	Phases	Sb_2O_5	As_2O_5	Al_2O_3	Fe_2O_3	SO_3	K_2O	Na_2O	SiO_2	CaO
Smelting waste	Fe (oxyhydr)oxides (n = 14)	6.01 (0.06–16.51)	(n.d.–0.63)	1.05 (0.23–3.39)	79.78 (65.03–98.65)	1.68 (0.01–8.40)	0.08 (0.02–0.25)	0.46 (0.01–2.90)	1.43 (0.17–5.27)	0.05 (0.01–0.15)
	Fe (oxyhydr)oxides: hematite (n = 5)	0.12 (0.06–0.26)	(n.d.–0.03)	1.16 (0.70–1.94)	96.39 (94.24–98.65)	0.04 (0.01–0.09)	n.d.	n.d.	1.04 (0.17–2.63)	0.05 (0.03–0.11)
	Jarosite-group minerals (natrojarosite) (n = 22)	1.43 (0.19–9.63)	0.07 (0.01–0.26)	1.14 (0.26–3.81)	42.12 (36.48–47.08)	25.51 (16.78–27.68)	0.58 (0.08–1.72)	7.63 (5.00–9.40)	0.37 (0.01–2.25)	0.04 (0.02–0.08)
	Reddish-black phases (Fe–Sb (oxyhydr)oxides) (n = 7)	30.59 (22.80–38.46)	0.91 (0.65–1.09)	1.40 (0.54–2.97)	44.35 (35.87–51.71)	3.73 (1.27–7.00)	0.22 (0.07–0.51)	0.94 (0.12–1.92)	5.70 (1.68–10.83)	(n.d.–0.08)
	Blackish-reddish-brown phases (tripuhyite) (n = 5)	53.33 (49.78–60.01)	1.67 (1.43–2.06)	0.59 (0.32–0.77)	34.49 (29.18–38.01)	1.35 (0.88–2.22)	(n.d.–0.04)	(n.d.–0.20)	2.90 (0.55–7.35)	(n.d.–0.73)

scorodite is usually less than 0.13 wt% Sb_2O_5, and the highest reported value is only 0.48 wt% Sb_2O_5 (Kossoff et al., 2015). Noticeable Sb concentrations were also found in phyllosilicates, with an average value of 2.15 wt% Sb_2O_5, whereas they contained trace amounts of As. Courtin-Nomade et al. (2012) suggested that minor amounts of Sb are likely to occur in some silicate minerals present in mine wastes.

Iron (oxyhydr)oxides in the mine tailings had an average Fe_2O_3 content of 90.27 wt% (which is very similar to the theoretical content in goethite, 89.86 wt%). These iron compounds contained 2.28 wt% Sb_2O_5 and 0.09 wt% As_2O_5 on average. The reddish-black phases showed the highest Sb content among this mine waste, with an average value of 18.64 wt% Sb_2O_5. These phases also had a significant Fe_2O_3 content (36.59 wt% on average). Their high Sb/Fe molar ratio (0.25) and the chemical heterogeneity revealed by BSE images suggest that these phases were mixtures of iron and antimony (oxyhydr)oxides, rather than iron (oxyhydr)oxides alone. Their As content was relatively low (0.58 wt% As_2O_5 on average). As in the mine waste rocks, phyllosilicates had an appreciable Sb content (1.30 wt% Sb_2O_5 on average) and trace levels of As.

The iron (oxyhydr)oxides in the smelting waste had a significant Sb content (up to 16.51 wt% Sb_2O_5), with an average value of 6.01 wt% Sb_2O_5; they had a much lower As content (up to 0.63 wt% As_2O_5). Among the iron (oxyhydr)oxides, hematite had the lowest Sb content (0.12 wt% Sb_2O_5 on average). The jarosite-group minerals, which were identified as natrojarosite by XRD, had a high Sb content (up to

9.63 wt% Sb_2O_5), with an average value of 1.43 wt% Sb_2O_5; they had a much lower As content (up to 0.26 wt% As_2O_5). These values are consistent with those found in jarosite $[KFe_3(SO_4)_2(OH)_6]$ in mine wastes resulting from the exploitation of other stibnite-bearing deposits (7.8 wt% Sb_2O_5 and 1.1 wt% As_2O_5 on average) (Courtin-Nomade et al., 2012). The retention of these two metalloids by jarosite proceeds differently. Whereas arsenate is retained by adsorption on the mineral surface (Savage et al., 2005; Asta et al., 2009) and, notably, by incorporation into the mineral structure to replace sulfate (Savage et al., 2005; Hudson-Edwards, 2019), most of the antimonate replaces octahedral Fe(III) in the mineral structure (Courtin-Nomade et al., 2012; Hudson-Edwards, 2019). The morphology of jarosite is not apparently affected by the incorporation of high Sb contents (Courtin-Nomade et al., 2012), whereas elevated As contents alter jarosite crystallinity (Savage et al., 2005). The reddish-black phases in these wastes, with characteristics suggesting they are mixtures of iron and antimony (oxyhydr)oxides, also had a very high Sb content (30.59 wt% Sb_2O_5 on average), a high Sb/Fe molar ratio (0.34), and a relatively low As content (0.91 wt% As_2O_5 on average). The blackish-reddish-brown phases had the highest Sb content (53.33 wt% Sb_2O_5 on average) and a significant Fe_2O_3 content (34.49 wt% on average); consequently, their Sb/Fe molar ratio was 0.76. This composition and the characteristics observed by polarized light microscopy suggest that these phases are tripuhyite. This weathering product has been found in waste in other mining areas with highly variable Sb and Fe contents

(5.49–55.16 wt% Sb_2O_5 and 22.79–72.67 wt% Fe_2O_3) (Majzlan et al., 2011; Courtin-Nomade et al., 2012; Lalinská-Voleková et al., 2012; Borčinová Radková et al., 2020). Other elements are also reportedly incorporated into the tripuhyite structure, such as As, Si, and Al (Lalinská-Voleková et al., 2012). This phase in the smelting waste contained 1.67 wt% As_2O_5, 2.90 wt% SiO_2, and 0.59 wt% Al_2O_3 on average.

The main phases acting as sinks of Sb in mine waste are tripuhyite, antimony (oxyhydr)oxides, iron (oxyhydr)oxides and natrojarosite. Also, iron (oxyhydr)oxides and natrojarosite together with Fe arsenates are the main responsible for immobilizing As. Under oxidizing conditions, tripuhyite and stibiconite (identified by XRD) are stable Sb phases within a wide range of pH conditions. Particularly, tripuhyite is considered the ultimate sink of Sb in these scenarios (Leverett et al., 2012), especially under low pH (Burton et al., 2020). Iron (oxyhydr)oxides are well known adsorbents of Sb and As, with low crystalline/amorphous compounds exhibiting the highest adsorption capacities. Additionally, these compounds can scavenge important amounts of these metalloids via co-precipitation (Waychunas et al., 1993; Ritchie et al., 2013; Kadokura et al., 2019). This is a significant route for attenuating their mobility in mining areas (Moldovan et al., 2003; Ritchie et al., 2013). Jarosite forms up to a pH of approximately 3 (Kendall et al., 2013; Cheng et al., 2009). The dissolution of jarosite releases Fe(III) and sulfate to solution, resulting in the formation of iron (oxyhydr)oxides and/or schwertmannite [$Fe_{16}O_{16}(OH)_{12}(SO_4)_2$] under moderate to high pH (Elwood Madden et al., 2012). The increasing As incorporation in jarosite results in short-term dissolution rate increases due to the bond polarization within the jarosite structure (Kendall et al., 2013; Hudson-Edwards, 2019). With time, an As enrichment on jarosite surface takes place because of the strong binding between arsenate and Fe(III), inhibiting jarosite dissolution (Kendall et al., 2013; Hudson-Edwards, 2019). Sulfides can induce the reductive dissolution of As-bearing jarosites, thus provoking the mobilization of As (Johnston et al., 2012). The reductive dissolution of As/Sb-bearing jarosites can also be induced by Fe(II). Thus, at pH of 5.5 the dissolution of jarosite is promoted by Fe(II). Under these conditions, Sb mobility increases prior to the formation of metastable green rust sulfate/goethite and the labile As fraction increases as well (Karimian et al., 2018). At pH of 7 the dissolution of jarosite is also promoted by Fe(II) and Sb is mobilized prior to the formation of green rust sulfate/goethite or lepidocrocite (γ-FeOOH). Likewise, an increase in the exchangeable fraction of As is produced (Karimian et al., 2017). Therefore, it could be expected that under variable geochemical conditions jarosites act as sinks for As and Sb at short time scales.

3.3. Environmental characterization

3.3.1. pH, EC, and NNP

The pH, EC, and NNP values of the mine waste are shown in Table 1. The mine waste rocks and mine tailings were alkaline, whereas the smelting waste were acidic, having a pH (3.4) in the range for acid-producing materials (pH < 4). The EC of the smelting waste (1270 μS cm^{-1}) was much higher than those of the mine waste rocks and mine tailings (253 and 117 μS cm^{-1}, respectively). The smelting waste was the only material with a negative NNP (-41.2 kg $CaCO_3$ t^{-1}), which is lower than the value (-30 kg $CaCO_3$ t^{-1}) below which a material is regarded in practice as potentially acid-producing. By contrast, the mine waste rocks and mine tailings showed high positive NNP values (194 and 446 kg $CaCO_3$ t^{-1}, respectively), which are characteristic of non-acid-producing materials (>30 kg $CaCO_3$ t^{-1}).

3.3.2. Leaching behavior and toxicity

Fig. 4 shows the leaching behavior of the mine waste determined according to the European leaching standard test EN-12457-4 (2002). The leachable Sb content in the mine waste followed the sequence mine waste rocks (28.4 mg kg^{-1}) > mine tailings (13.7 mg kg^{-1}) > smelting waste (1.05 mg kg^{-1}). These values represent small fractions of the total Sb, within the range 1.2–0.002%, where the smelting waste had the lowest fraction. All three types of waste had leachable Sb contents above the limit for acceptance at non-hazardous waste landfills (0.7 mg kg^{-1}) established by Council Decision 2003/33/EC (European Council Decision, 2003) on the criteria and procedures for the acceptance of waste at landfills. Moreover, the leachable Sb content of the mine waste rocks and mine tailings greatly exceeded the limit for acceptance at hazardous waste landfills (5 mg kg^{-1}) [Council Decision 2003/33/EC (European Council Decision, 2003)]. Therefore, the mine waste rocks and mine tailings must be stabilized or encapsulated to meet the controlled landfill acceptance criteria for Sb leaching. By contrast, the leachable As content of the mine waste was low (< 0.5–1.17 mg kg^{-1}) and meets the criteria for acceptance at non-hazardous waste landfills (2 mg kg^{-1}) [Council Decision 2003/33/EC (European Council Decision, 2003)]. The leachable sulfate content varied significantly with the type of mine waste. The value for smelting waste (21,900 mg kg^{-1}) was approximately two orders of magnitude higher than those for mine waste rocks (285 mg kg^{-1}) and mine tailings (79.4 mg kg^{-1}) and exceeds the limit for acceptance at non-hazardous waste landfills (20,000 mg kg^{-1}) [Council Decision 2003/33/EC (European Council Decision, 2003)].

Fig. 4 also shows the results of the TCLP test used to determine the toxicity of the mine waste. The Sb concentration in leachates released from the mine waste followed the sequence mine waste rocks (6.86 mg L^{-1}) > mine tailings (2.02 mg L^{-1}) > smelting waste (1.05 mg L^{-1}). All these values exceed the threshold (0.6 mg L^{-1}) for the characterization of wastes as toxic, which was set at 100 times the drinking water standard of the United States Environmental Protection Agency (US EPA) (Guo et al., 2014). Therefore, measures should be undertaken to decrease the Sb release from this waste and reduce its toxicity. The As concentration in leachates released from the mine waste was low (<0.05 mg L^{-1}) and was well below the TCLP regulatory limit (5 mg L^{-1}).

3.3.3. Effect of competing anions

The effect of competing anions on the desorption of Sb and As from the mine waste is shown in Fig. 5. In the smelting waste, the occurrence of Sb in adsorbed forms via either outer- or inner-sphere complexes was almost negligible (0.002 and 0.007% of the total content, respectively). The mine waste rocks and mine tailings both contained notable amounts of adsorbed Sb, especially in specifically adsorbed forms (0.58 and 0.62% of the total content, respectively), whereas non-specifically adsorbed Sb was present in smaller amounts (0.13 and 0.14% of the total content, respectively). Therefore, the introduction of anions competing for the adsorption sites in these mine waste systems represents a limited risk of further Sb mobilization, which is almost negligible for the smelting waste and relatively low for the mine waste rocks and mine tailings. Various geological materials can be good adsorbents for Sb, including clay minerals (Xi et al., 2010, 2014, 2016; Ilgen and Trainor, 2012; Rakshit et al., 2015), layered double hydroxides (LDHs) (Dore and Frau, 2018; Dore et al., 2019), iron hydroxy sulfates (Dong et al., 2015; Li et al., 2016), and Fe, Al, and Mn (oxyhydr)oxides (Thanabalasingam and Pickering, 1990; Kolbe et al., 2011; Rakshit et al., 2015; Ilgen and Trainor, 2012; Sun et al., 2019). Kaolinite is the most extensively studied clay mineral. Antimony is strongly adsorbed on kaolinite in an inner-sphere mode, forming mostly bidentate complexes (Ilgen and Trainor, 2012), although the formation of outer-sphere complexes has also been suggested in the removal of its oxidized form under alkaline conditions (Xi et al., 2010). Antimony adsorption on kaolinite depends significantly on pH (Xi et al., 2010, 2016; Rakshit et al., 2015) and decreases at pH values above approximately 3.5–4 (Xi et al., 2010). Competitive anions reportedly have only a negative effect on the adsorption of antimonate, which is especially remarkable at high pH (Xi et al., 2010, 2014). In contrast to kaolinite, LDHs are well able to remove antimonate at circumneutral pH (Dore and Frau, 2018). It is retained by the formation of brandholzite-like compounds
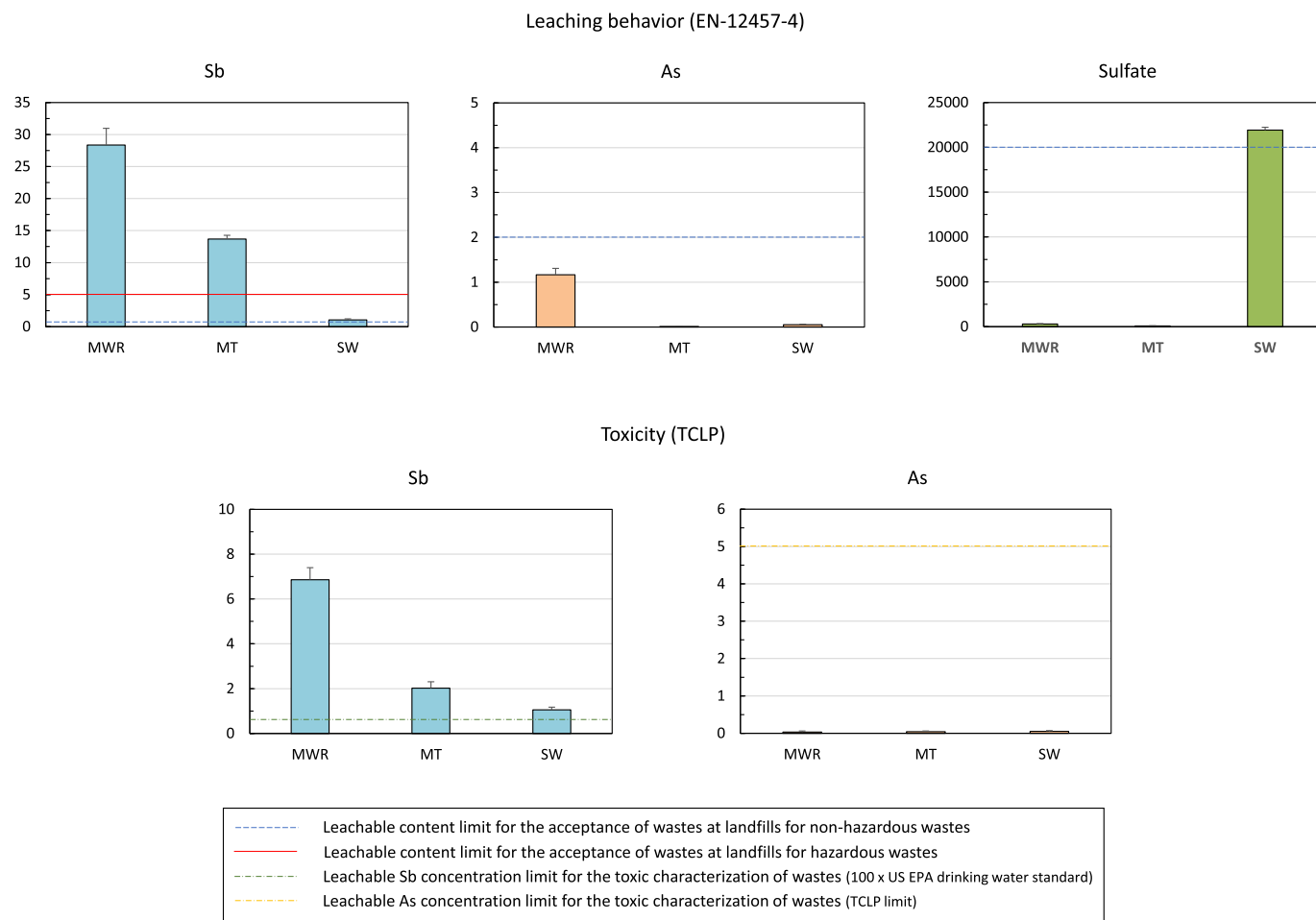
Fig. 4. Leaching behavior and toxicity of mine wastes (MWR: mine waste rocks, MT: mine tailings, and SW: smelting waste).
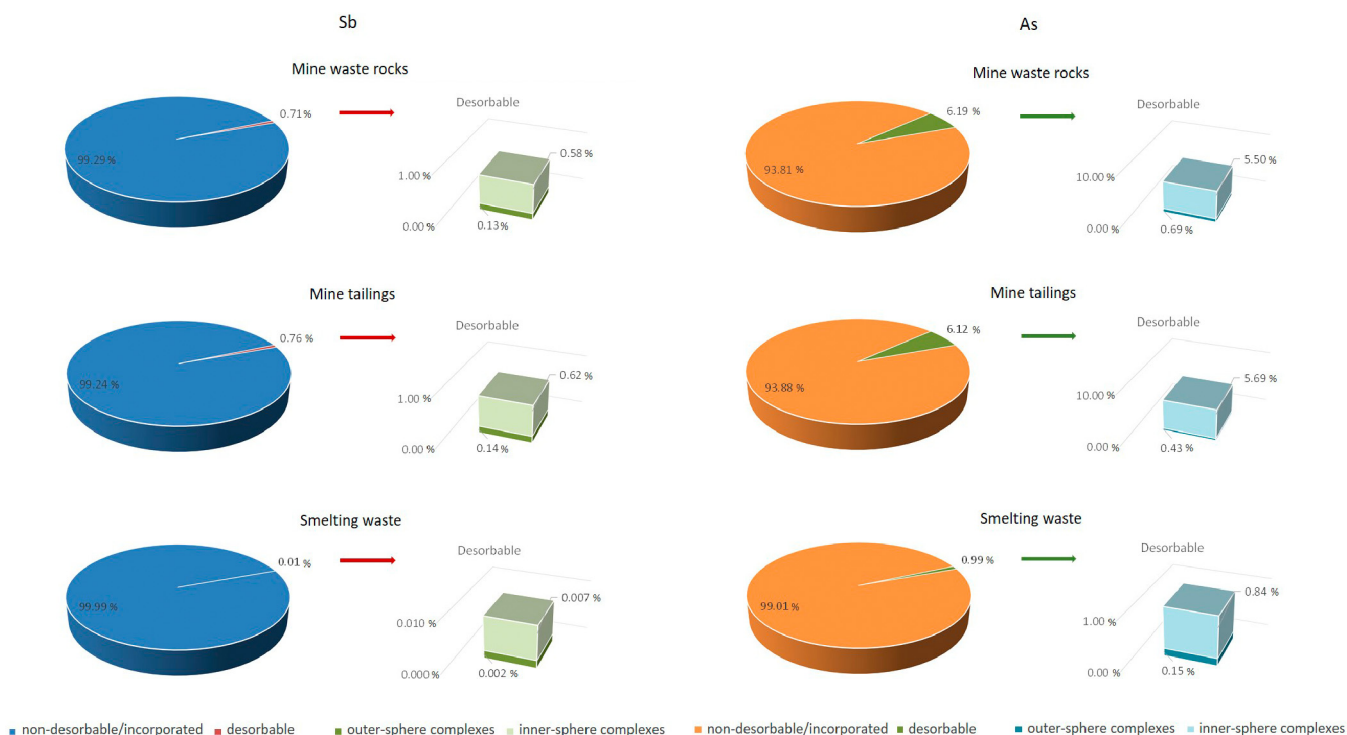

**Fig. 5.** Antimony and arsenic desorbable fractions in mine wastes.

by the uncalcined nitrate Mg/Al LDH and calcined carbonate Mg/Al LDH (Dore and Frau, 2018). When Mg is replaced by Zn in the calcined carbonate LDH, antimonate enters the interlayer, and thus the LDH structure is reconstructed (Dore and Frau, 2018). The calcined products show better removal efficiencies, which are only slightly or moderately decreased by the presence of competing anions, except for arsenate, which strongly affects the removal efficiency (Dore et al., 2019). However, various calcined LDHs can significantly decrease the Sb content of mine drainage while simultaneously removing much of the As (Dore et al., 2019). Consequently, they could be promising adsorbents for this application. Iron hydroxy sulfates such as jarosite and schwertmannite are important weathering phases in mining environments and have been found to scavenge Sb (Harris et al., 2003; Manaka et al., 2007; Courtin-Nomade et al., 2012). In particular, schwertmannite can reduce the Sb content significantly by adsorption (Dong et al., 2015; Li et al., 2016) via anion exchange between sulfate and antimonate (Dong et al., 2015). Moreover, this adsorption decreases only slightly at pH values above approximately 6 and in the presence of competing anions, except for silicate and carbonate, which cause moderate and high decreases in adsorption, respectively (Dong et al., 2015). However, schwertmannite is a metastable phase and is easily transformed into goethite (Zhang et al., 2018). Therefore, schwertmannite can be expected to decrease Sb mobility only at short time scales. Antimony is adsorbed by metal (oxyhydr)oxides mainly by the formation of inner-sphere complexes (Leuz et al., 2006; Mitsunobu et al., 2010; Ilgen and Trainor, 2012). These compounds adsorb Sb over a wide pH range when it is present in its reduced form, whereas the adsorption of antimonate is significantly reduced under neutral and alkaline conditions (Wilson et al., 2010). Competing anions can cause some Sb desorption from these surfaces, with phosphate showing the strongest effect (Biver et al., 2011). Less-effective competing anions generally have little effect on Sb desorption from Fe (oxyhydr)oxides, which is thus unaffected or only slightly affected by them (Biver et al., 2011). This behavior is especially significant in mining environments where Fe (oxyhydr)oxides generally dominate and significant amounts of dissolved sulfate are released from oxidizing sulfides. Moreover, it was recently reported that over time, Sb adsorbed on amorphous/poorly crystalline Fe oxides is transformed into incorporated Sb, likely by micropore diffusion and/or by the substitution of antimonate for surface octahedral Fe(III) in these compounds (Verbeeck et al., 2021). This process, together with the structural incorporation of antimonate within Fe (oxyhydr)oxides by co-precipitation (Mitsunobu et al., 2010), may represent important pathways for decreasing Sb mobility in these scenarios. These mitigation processes may control Sb mobility on relatively long time scales, unless reducing conditions are established. Under reducing conditions, the dissolution of amorphous/poorly crystalline Fe oxides occurs, although crystalline Fe compounds are generally more resistant to this dissolution process (Keon et al., 2001). The adsorption of antimonate on crystalline Fe compounds such as goethite is also reportedly shifted to partial incorporation of antimonate into the mineral structure to replace Fe(III) (Burton et al., 2020). This process is mediated by the occurrence of Fe (II) in solution, which causes rapid goethite recrystallization; it increases the total amount of adsorbed Sb while decreasing the desorbable Sb fraction (Burton et al., 2020). In addition, this Fe(II)-catalyzed recrystallization process may result in the formation of tripuhyite (Leverett et al., 2012). Tripuhyite is thermodynamically favored over goethite at low pH; however, at near-neutral pH and aqueous antimonate concentrations below approximately 600 μM, goethite is favored over tripuhyite (Burton et al., 2020). Both the incorporation of antimonate into the goethite structure and the formation of tripuhyite can significantly reduce Sb mobility in mine environments on long time scales.

Adsorbed forms of As were present in larger amounts than adsorbed Sb. Thus, in the smelting waste, adsorbed As represented approximately 1% of the total As (0.15% formed outer-sphere complexes, and 0.84% formed inner-sphere complexes). Adsorbed As was also more common in the mine waste rocks and mine tailings, in particular specifically

adsorbed forms (5.50 and 5.69% of the total content, respectively), whereas non-specifically adsorbed As was less abundant (0.69 and 0.43% of the total content, respectively). Therefore, relatively large amounts of As, unlike Sb, can be mobilized by the introduction of anions competing for adsorption sites in these mine waste systems, particularly mine waste rocks and mine tailings. Clay minerals, LDHs, iron hydroxy sulfates, and metal (oxyhydr)oxides also adsorb As. This metalloid in its oxidized state is better adsorbed by clay minerals, and its adsorption decreases considerably above neutral pH (Lin and Puls, 2000). Arsenic is generally adsorbed by variable charges in clay minerals at their broken bonds or edges (Wilson et al., 2010). Both calcined and uncalcined LDHs have been shown to adsorb As (Gillman, 2006; Türk et al., 2020). In particular, the occurrence of sulfate Zn-Cu/Al LDHs in several mining scenarios has been reported (Ardau et al., 2011). These LDHs show very high affinity for As. This metalloid is adsorbed in the interlayer space through exchange with sulfate, but the actual role of these phases in natural attenuation processes is not clear (Ardau et al., 2011). By contrast, iron hydroxy sulfates are important sinks of this metalloid. Adsorption plays an important role in As removal by these phases. Thus, jarosite and schwertmannite can adsorb As on their surfaces through the formation of inner-sphere bidentate binuclear complexes (Gräfe et al., 2008; Paikaray et al., 2014). Arsenic adsorption on metal (oxyhydr)oxides also occurs mainly by the formation of inner-sphere bidentate binuclear complexes, although outer-sphere complexes can also be formed on poorly crystalline/amorphous Fe compounds and on crystalline and amorphous Al compounds when As is present in its reduced state, where most outer-sphere complexes are formed on amorphous Al compounds (Waychunas et al., 1993; Gräfe et al., 2008; Wang and Mulligan, 2008). The adsorption of As on Fe and Al (oxyhydr)oxides depends strongly on pH; it is maximum in the oxidized state of As at pH 2–6 and decreases at higher pH, whereas the adsorption of the reduced form is greatest above this pH range (Wang and Mulligan, 2006; Lee et al., 2014; Álvarez-Ayuso and Murciego, 2021). Among competing anions, phosphate strongly outcompetes As for adsorption sites on various materials, especially when As is in its oxidized state (Manning and Goldberg, 1996; Jain and Loeppert, 2000; Lin and Puls, 2000). The presence of both As and Sb also affects the adsorption process, where arsenate adsorption is clearly favored over antimonate adsorption (Kolbe et al., 2011; Fawcett et al., 2015). However, in the mine waste considered here, Sb is much more abundant than As, and thus this type of differential adsorption has no appreciable effect.

3.3.4. Chemical fractionation

Fig. 6 shows the chemical fractionation of Sb and As, which was determined following the modified BCR protocol described by Rauret et al. (1999). According to the sequential extraction procedure, the distribution of Sb in each fraction of the different types of mine waste followed the order residual ≫ reducible > oxidizable > acid-soluble. Antimony is largely distributed in the residual fraction, with values of 94.1, 93.6, and 99.9% in the mine waste rocks, mine tailings, and smelting waste, respectively. The Sb distribution in the other fractions of the smelting waste was quite low (<0.1%), indicating a relatively limited risk of further Sb mobilization from the smelting waste under changing environmental conditions. By contrast, reducing conditions, under which amorphous/poorly crystalline iron oxides dissolve, would result in the mobilization of up to 4.6 and 3.3% of the total Sb content in the mine waste rocks and mine tailings, respectively. The Sb portion of their oxidizable fractions was 1.0 and 2.3%, respectively, whereas that of their acid-soluble fractions was less than 1%. Therefore, although the eventual acidification of this mine waste would mobilize some Sb, it poses a lower risk of Sb release into the environment than changes in the redox conditions. The acid-soluble fraction is thought to be the most bioavailable fraction and thus represents the greatest hazard to the environment (Pérez-López et al., 2008). To identify the environmental risk posed by wastes, the following criteria for the acid-soluble fraction value obtained using the BCR protocol has been proposed: low risk

Sb

As

■ Acid-soluble □ Reducible ▨ Oxidizable ▨ Residual
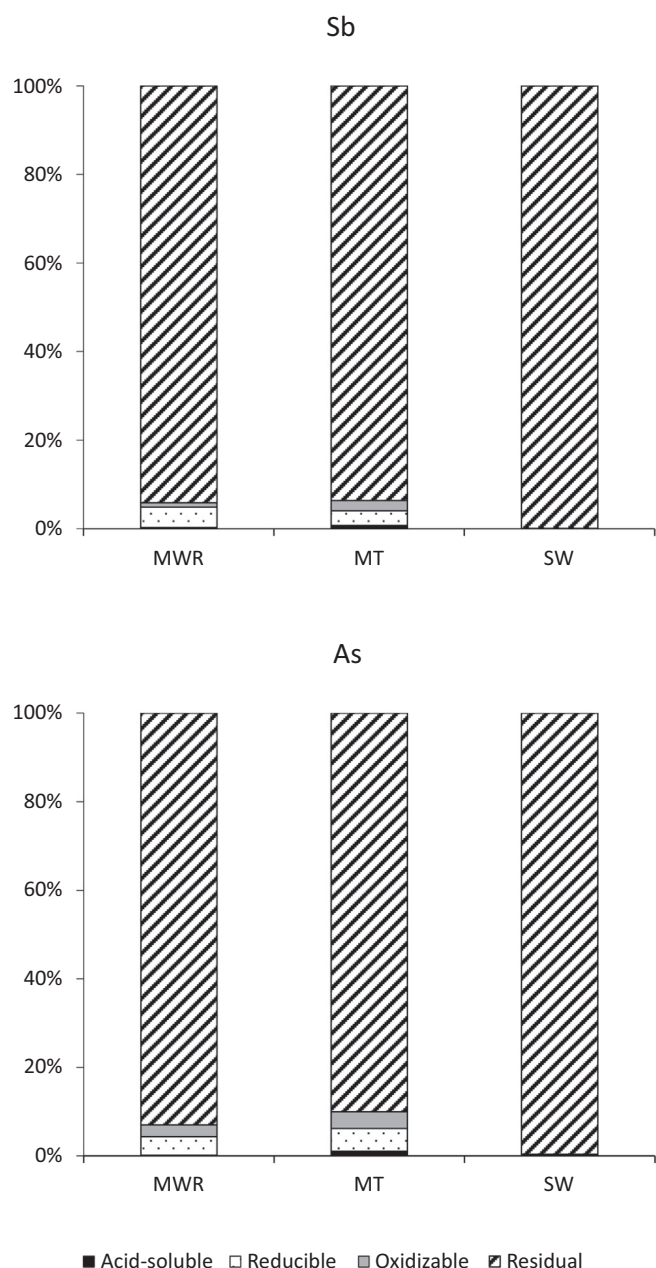
Fig. 6. Partitioning of Sb and As between the acid-soluble, reducible, oxidizable, and residual fractions of mine wastes (MWR: mine waste rocks, MT: mine tailings, and SW: smelting waste).

(<1%), moderate risk (>1% and <10%), high risk (>10% and <50%), and very high risk (>50%) (Guo et al., 2014). According to these criteria, this mine waste would pose a low risk of Sb exposure in terms of the total content.

In the sequential extraction procedure, the As partitioning in each fraction of the mine wastes also followed the sequence residual ≫ reducible > oxidizable > acid-soluble. The As distribution in the residual fraction was 92.9, 90.0, and 99.6% in the mine waste rocks, mine tailings, and smelting waste, respectively. The As portion of the other fractions of the smelting waste was low (<0.1% in the acid-soluble and reducible fractions and <0.3% in the oxidable fraction), suggesting a low risk of further As mobilization under changing environmental conditions. By contrast, reducing conditions could mobilize up to 4.2 and 5.1% of the total As content in the mine waste rocks and mine tailings, respectively. The As portion of their oxidizable fraction was 2.7 and 3.8%, respectively, and that of their acid-soluble fraction was approximately 0.1 and 1%,

respectively. Like Sb, As is more likely to be released from the mine waste rocks and mine tailings by changes in the redox conditions (the establishment of reducing conditions, under which amorphous/poorly crystalline iron oxides dissolve, or the development of oxidation processes) than by possible acidification processes. According to the above criteria for identifying the environmental risk posed by wastes, the risk of As exposure can also be considered low in terms of its total content. Moreover, acid events are unlikely to affect the mine waste rocks and mine tailings because of their high acid-buffering capacity.

3.4. Analysis of water samples

The parameters measured in water samples are indicated in Table 3. All water types showed slightly alkaline pH (7.7–8.0), attributable to the buffering capacity of abundant carbonates. The water EC varied within the range 160–813 $\mu S \ cm^{-1}$, and well and pond waters had the highest values. Alkalinity ranged from 21 to 130 mg $CaCO_3 \ L^{-1}$. Almost all water samples were Ca-dominated. The concentration of Fe showed low values (<1 mg L^{-1}) and is consistent with the very low solubility of Fe(III) under neutral or alkaline conditions because of its precipitation as Fe (oxyhydr)oxides. Moreover, Fe(II) is quickly oxidized at near-neutral pH and subsequently precipitated (Casiot et al., 2005). The highest S concentration (59 mg L^{-1}) was found in the pond near the area of deposition of mine wastes. This pond has received more directly the impact of sulfide weathering processes and dissolution/transformation reactions of iron hydroxy sulfates. The S concentration in the other water samples remained <4 mg L^{-1}. The Sb concentration in most water samples remained <1 $\mu g \ L^{-1}$, similar to those typically found in fresh waters (1 $\mu g \ L^{-1}$) (Filella et al., 2002). Slightly increased Sb concentrations were attained in well and river waters collected downstream the mine site (1.7 and 2.4 $\mu g \ L^{-1}$, respectively). By contrast, the Sb concentration in the pond nearest the mine site reached a value of 89 $\mu g \ L^{-1}$, greatly exceeding the WHO (20 $\mu g \ L^{-1}$) and EPA (6 $\mu g \ L^{-1}$) drinking water standards. The As concentration was <1 $\mu g \ L^{-1}$ in streams and in the range of 1.6–22.1 $\mu g \ L^{-1}$ in well and pond waters. The highest As concentration was found in the pond nearest the mine site, exceeding the WHO (10 $\mu g \ L^{-1}$) and EPA (10 $\mu g \ L^{-1}$) drinking water standards. The As concentration in the other water bodies was within the typical range of fresh waters (1–10 $\mu g \ L^{-1}$) (Mandal and Suzuki, 2002). Water analyses reveal relatively little remobilization of Sb and As downstream the mine site.

4. Conclusions

The characterization of weathered mine wastes derived from the exploitation of stibnite ore deposits revealed the important effects of the deposit mineralogy, applied Sb recovery process, established pH conditions, and elemental availability on the occurrence of Sb-bearing weathering products and the risk of Sb mobilization from these products. The Sb distribution and mobility in the mine waste varied depending on these factors.

The mine waste rocks and mine tailings were composed mainly of silicate and carbonate minerals of the bedrock hosting the mineralized system. These minerals, especially the latter, were responsible for the acid-neutralizing capacity and alkaline nature of the mine waste rocks and mine tailings. Their phyllosilicates had noticeable Sb contents (2.15 and 1.30 wt% Sb_2O_5 on average, respectively). Additionally, sulfide weathering products, although rare, reduced the release of Sb. Iron (oxyhydr)oxides (2.28–5.97 wt% Sb_2O_5 on average) and/or mixtures of iron and antimony (oxyhydr)oxides were the most significant. Most of the Sb in the mine waste rocks and mine tailings was present in the residual fraction. However, this mine waste is not acceptable at hazardous waste landfills because of its leachable Sb content, and thus it requires prior stabilization or encapsulation. The introduction of competing anions or the occurrence of acidification processes could mobilize Sb at relatively low levels (<0.8 and <1% of

Table 3
Element concentrations, pH, EC, and alkalinity of waters.

Parameter	C1	C2	R1a	R1b	P1	P2	P3	W1
Sb ($\mu g\ L^{-1}$)	<1	<1	<1	2.4	89	<1	<1	1.7
As ($\mu g\ L^{-1}$)	<1	<1	<1	<1	22.1	1.6	2.0	1.8
Ca ($mg\ L^{-1}$)	9.2	19.8	22.3	22.5	96	27.2	24.6	63
Fe ($mg\ L^{-1}$)	<0.5	0.94	<0.5	<0.5	<0.5	<0.5	0.62	<0.5
K ($mg\ L^{-1}$)	0.57	1.8	<0.5	<0.5	3.1	5.7	1.2	0.50
Mg ($mg\ L^{-1}$)	7.4	7.7	11.5	11.4	46	11.9	5.6	11.9
Mn ($mg\ L^{-1}$)	<0.5	<0.5	<0.5	<0.5	<0.5	<0.5	3.3	<0.5
Na ($mg\ L^{-1}$)	11.5	9.0	7.1	7.3	31	15.4	8.1	14.0
S ($mg\ L^{-1}$)	2.3	1.7	2.1	2.2	59	1.1	3.2	3.6
pH	8.0	7.8	7.9	8.0	7.9	7.8	7.7	8.0
EC ($\mu S\ cm^{-1}$)	160	190	213	220	813	303	203	417
Alk ($mg\ CaCO_3\ L^{-1}$)	21	40	47	47	130	61	36	87

the total Sb content, respectively), whereas the establishment of reducing conditions, under which amorphous/poorly crystalline iron oxides dissolves, poses a higher risk of further Sb mobilization (4.6 and 3.3% of the total Sb content of mine waste rocks and mine tailings, respectively).

The smelting waste produced by treatment for the recovery of Sb from ore was characterized by acidity and a significant Sb content (4.72%). Additionally, Fe was also present at high concentrations, facilitating the formation of various Fe compounds that would greatly decrease Sb release. Thus, natrojarosite (with 1.43 wt% Sb_2O_5 on average), iron (oxyhydr)oxides (with 6.01 wt% Sb_2O_5 on average), mixtures of iron and antimony (oxyhydr)oxides, and tripuhyite were present. Almost all the Sb in the smelting waste was present in the residual fraction. The Sb leachable content (<2 mg kg^{-1}) of the smelting waste was a very small fraction (0.002%) of the total Sb and was within the limit for acceptance at hazardous waste landfills. Similarly, the amount of Sb in desorbable forms and the amount that could be mobilized under reducing conditions accounted for small fractions of the total content (<0.01 and <0.1%, respectively). Thus, if present acid conditions continue, the risk of further Sb release from the smelting waste under changing environmental conditions can be considered very low.

The As content of each type of mine waste was low, and the leachable As content did not reach toxic or hazardous levels. The main weathering products acting as sinks for As were AFA and iron (oxyhydr)oxides. Further mobilization could occur, especially from mine waste rocks and mine tailings, in the presence of anions competing for adsorption sites (approximately 6% of total As) or under reducing conditions (approximately 4–5% of total As).

CRediT authorship contribution statement

E. Álvarez-Ayuso: Conceptualization, Investigation, Writing – review & editing. **A. Murciego:** Investigation. **M.A. Rodríguez:** Resources. **L. Fernández-Pozo:** Resources. **J. Cabezas:** Contribution to funding acquisition. **J.M. Naranjo-Gómez:** Contribution to funding acquisition. **R. Mosser-Ruck:** Contribution to funding acquisition.

Declaration of competing interest

The authors declare that they have no known competing financial interests or personal relationships that could have appeared to influence the work reported in this paper.

Acknowledgments

References

Ackermann, S., Gieré, R., Newville, M., Majzlan, J., 2009. Antimony sinks in the weathering crust of bullets from Swiss shooting ranges. Sci. Total Environ. 407, 1669–1682.

Alloway, B.J., 1995. Heavy Metals in Soils. Blackie Academic & Professional, Glasgow.

Álvarez-Ayuso, E., Murciego, A., 2021. Stabilization methods for the treatment of weathered arsenopyrite mine wastes: arsenic immobilization under selective leaching conditions. J. Clean. Prod. 283, 125265.

Álvarez-Valero, A.M., Sáez, R., Pérez-López, R., Delgado, J., Nieto, J.M., 2009. Evaluation of heavy metal bio-availability from Almagrera pyrite-rich tailings dam (Iberian Pyrite Belt, SW Spain) based on a sequential extraction procedure. J. Geochem. Explor. 102, 87–94.

Anderson, C.G., 2001. Hydrometallurgically treating antimony-bearing industrial wastes. JOM 53, 18–20.

Ardau, C., Cannas, C., Fantauzzi, M., Rossi, A., Fanfani, L., 2011. Arsenic removal from surface waters by hydrotalcite-like sulphate minerals: field evidences from an old mine in Sardinia, Italy. Neues Jahrb. für Mineral. Abhandlungen 188, 49–63.

Ashley, P.M., Craw, D., Graham, B.P., Chappell, D.A., 2003. Environmental mobility of antimony around mesothermal stibnite deposits, New South Wales, Australia and southern New Zealand. J. Geochem. Explor. 77, 1–14.

Asta, M.P., Cama, J., Martínez, M., Giménez, J., 2009. Arsenic removal by goethite and jarosite in acidic conditions and its environmental implications. J. Hazard. Mater. 171, 965–972.

Baroni, F., Boscagli, A., Protano, G., Riccobono, F., 2000. Antimony accumulation in *Achillea ageratum*, *Plantago lanceolata* and *Silene vulgaris* growing in an old Sb-mining area. Environ. Pollut. 109, 347–352.

Beauchemin, S., Kwong, Y.T.J., Desbarats, A.J., MacKinnon, T., Percival, J.B., Parsons, M.B., Pandya, K., 2012. Downstream changes in antimony and arsenic speciation in sediments at a mesothermal gold deposit in British Columbia, Canada. Appl. Geochem. 27, 1953–1965.

Biddau, R., Cidu, R., 2017. Metals and metalloids in wild asparagus at uncontaminated and mining-contaminated sites. J. Environ. Qual. 46, 320–329.

Biver, M., Krachler, M., Shotyk, W., 2011. The desorption of antimony(V) from sediments, hydrous oxides, and clay minerals by carbonate, phosphate, sulfate, nitrate, and chloride. J. Environ. Qual. 40, 1143–1152.

Biver, M., Shotyk, W., 2012. Stibnite (Sb_2S_3) oxidative dissolution kinetics from pH 1 to 11. Geochim. Cosmochim. Acta 79, 127–139.

Biver, M., Shotyk, W., 2013. Stibiconite (Sb_3O_6OH), senarmontite (Sb_2O_3) and valentinite (Sb_2O_3): dissolution rates at pH 2–11 and isoelectric points. Geochim. Cosmochim. Acta 109, 268–279.

Boreiko, C.J., Rossman, T.G., 2020. Antimony and its compounds: health impacts related to pulmonary toxicity, cancer, and genotoxicity. Toxicol. Appl. Pharmacol. 403, 115156.

Borčinová Radková, A., Jamieson, H.E., Campbell, K.M., 2020. Antimony mobility during the early stages of stibnite weathering in tailings at the Beaver Brook Sb deposit, Newfoundland. Appl. Geochem. 115, 104528.

Burton, E.D., Hockmann, K., Karimian, N., 2020. Antimony sorption to goethite: effects of Fe(II)-catalyzed recrystallization. ACS Earth Space Chem. 4, 476–487.

Cappuyns, V., Van Campen, A., Helser, J., 2021. Antimony leaching from soils and mine waste from the Mau Due antimony mine, North-Vietnam. J. Geochem. Explor. 220, 106663.

Casiot, C., Lebrun, S., Morin, G., Bruneel, O., Personné, J.C., Elbaz-Poulichet, F., 2005. Sorption and redox processes controlling arsenic fate and transport in a stream impacted by acid mine drainage. Sci. Total Environ. 347, 122–130.

Cheng, H., Hu, Y., Luo, J., Xu, B., Zhao, J., 2009. Geochemical processes controlling fate and transport of arsenic in acid mine drainage (AMD) and natural systems. J. Hazard. Mater. 165, 13–26.

Cidu, R., Biddau, R., Dore, E., Vacca, A., Marini, L., 2014. Antimony in the soil-water-plant system at the Su Suergiu abandoned mine (Sardinia, Italy): strategies to mitigate contamination. Sci. Total Environ. 497–498, 319–331.

Cooper, R., Harrison, A., 2009. The exposure to and health effects of antimony. Indian J. Occup. Environ. Med. 13, 3–10.

Courtin-Nomade, A., Rakotoarisoa, O., Bril, H., Grybosa, M., Forestier, L., Foucher, F., Kunz, M., 2012. Weathering of Sb-rich mining and smelting residues: insight in solid speciation and soil bacteria toxicity. Chem. Erde Geochem. 72 (S4), 29–39.

Courtin-Nomade, A., Waltzing, T., Evrard, C., Soubrand, M., Lenain, J.-F., Ducloux, E., Ghorbel, S., Grosbois, C., Bril, H., 2016. Arsenic and lead mobility: from tailing materials to the aqueous compartment. Appl. Geochem. 64, 10–21.

Craw, D., Wilson, N., Ashley, P.M., 2004. Geochemical controls on the environmental mobility of Sb and As at mesothermal antimony and gold deposits. Trans. Inst. Min. Metall. B: Appl. Earth Sci. 113, B3–B10.

Diemar, G.A., Filella, M., Leverett, P., Williams, P.A., 2009. Dispersion of antimony from oxidizing ore deposits. Pure Appl. Chem. 81, 1547–1553.

Dong, S., Dou, X., Mohan, D., Pittman, C.U., Luo, J., 2015. Synthesis of graphene oxide/schwertmannite nanocomposites and their application in Sb(V) adsorption from water. Chem. Eng. J. 270, 205–214.

Dordević, T., Kolitsch, U., Serafimovski, T., Tasev, G., Tepe, N., Stoger-Pollach, M., Hofmann, T., Boev, B., 2019. Mineralogy and weathering of realgar-rich tailings at a former As-Sb-Cr mine at Lojane, North Macedonia. Can. Mineral. 57, 403–423.

Dore, E., Frau, F., 2018. Antimonate uptake by calcined and uncalcined layered double hydroxides: effect of cationic composition and M²⁺/M³⁺ molar ratio. Environ. Sci. Pollut. Res. 25, 916–929.

Dore, E., Frau, F., Cidu, R., 2019. Antimonate removal from polluted mining water by calcined layered double hydroxides. Crystals 9, 410.

Dos Santos, E.C., Lourenço, M.P., Pettersson, L.G.M., Duarte, H.A., 2017. Stability, structure, and electronic properties of the pyrite/arsenopyrite solid-solid interface-a DFT study. J. Phys. Chem. C 121, 8042–8051.

Druzbicka, J., Craw, D., 2015. Metalloid attenuation from runoff waters at an historic orogenic gold mine, New Zealand. Mine Water Environ. 34, 417–429.

Dupont, D., Arnout, S., Jones, P.T., Binnemans, K., 2016. Antimony recovery from end-of-life products and industrial process residues: a critical review. J. Sustain. Met. 2, 79–103.

Elwood Madden, M.E., Madden, A.S., Rimstidt, J.D., Zahrai, S., Kendall, M.R., Miller, M.A., 2012. Jarosite dissolution rates and nanoscale mineralogy. Geochim. Cosmochim. Acta 91, 306–321.

EN-12457-4, 2002. Characterization of Waste - Leaching-Compliance Test for Leaching of Granular Waste Materials and Sludges - Part 4: One Stage Batch Test at a Liquid to Solid Ratio of 10 L/kg for Materials With Particle Size Below 10 mm (Without or With Size Reduction). European Committee for Standardization, Brussels.

European Council Decision, 2003. Council Decision 2003/33/EC of 19 December 2002 establishing criteria and procedures for the acceptance of waste at landfills pursuant to Article 16 of and Annex II to Directive 1999/31/EC. Off. J. Eur. Commun. L11, 27–49.

Fawcett, S.E., Jamieson, H.E., Nordstrom, D.K., McCleskey, R.B., 2015. Arsenic and antimony geochemistry of mine wastes, associated waters and sediments at the Giant Mine, Yellowknife, Northwest Territories, Canada. Appl. Geochem. 62, 3–17.

Feng, R., Wei, C., Tu, S., Ding, Y., Wang, R., Guo, J., 2013. The uptake and detoxification of antimony by plants: a review. Environ. Exp. Bot. 96, 28–34.

Feng, R., Liao, G.J., Guo, J.K., Wang, R.G., Xu, Y.M., Ding, Y.Z., Mo, L.Y., Fan, Z.L., Li, N.Y., 2016. Responses of root growth and antioxidative systems of paddy rice exposed to antimony and selenium. Environ. Exp. Bot. 122, 29–38.

Filella, M., Belzile, N., Chen, Y.-W., 2002. Antimony in the environment: a review focused on natural waters I. Occurrence. Earth Sci. Rev. 57, 125–176.

Filella, M., Belzile, N., Lett, M.-C., 2007. Antimony in the environment: a review focused on natural waters. III. Microbiota relevant interactions. Earth Sci. Rev. 80, 195–217.

Filella, M., Philippo, S., Belzile, N., Chen, Y., Quentel, F., 2009. Natural attenuation processes applying to antimony: a study in the abandoned antimony mine in Goesdorf, Luxembourg. Sci. Total Environ. 407, 6205–6216.

Flaková, R., Ženišová, Z., Krčmár, D., Ondrejková, I., Sracek, O., 2017. Occurrence of antimony and arsenic at mining sites in Slovakia: implications for their mobility. Carpathian J. Earth Environ. Sci. 12, 41–48.

Flakova, R., Zenisova, Z., Sracek, O., Krcmar, D., Ondrejkova, I., Chovan, M., Lalinská, B., Fendekova, M., 2012. The behavior of arsenic and antimony at Pezinok mining site, southwestern part of the Slovak Republic. Environ. Earth Sci. 66, 1043–1057.

Gillman, G.P., 2006. A simple technology for arsenic removal from drinking water using hydrotalcite. Sci. Total Environ. 366, 926–931.

Gräfe, M., Beattie, D.A., Smith, E., Skinner, W.M., Singh, B., 2008. Copper and arsenate co-sorption at the mineral-water interfaces of goethite and jarosite. J. Colloid Interface Sci. 322, 399–413.

Gumiel, P., Arribas, A., 1987. Antimony deposits in the Iberian Peninsula. Econ. Geol. 82, 1453–1463.

Gumiel, P., Campos, R., Monteserín, V., Bellido, F., 2002. Mapa Geológico y de Recursos Minerales del Sector Centro-Occidental de Extremadura (escala 1:100.000). Junta de Extremadura.

Guo, X., Wang, K., He, M., Liu, Z., Yang, H., Li, S., 2014. Antimony smelting process generating solid wastes and dust: characterization and leaching behaviors. J. Environ. Sci. (China) 26, 1549–1556.

Harris, D.L., Lottermoser, B.G., Duchesne, J., 2003. Ephemeral acid mine drainage at the Montalbion silver mine, north Queensland. Aust. J. Earth Sci. 50, 797–809.

He, M., Wang, N., Long, X., Zhang, C., Ma, C., Zhong, Q., Wang, A., Wang, Y., Pervaiz, A., Shan, J., 2019. Antimony speciation in the environment: recent advances in understanding the biogeochemical processes and ecological effects. J. Environ. Sci. (China) 75, 14–39.

Herath, I., Vithanage, M., Bundschuh, J., 2017. Antimony as a global dilemma: geochemistry, mobility, fate and transport. Environ. Pollut. 223, 545–559.

Hiller, E., Lalinská, B., Chovan, M., Jurkovič, Ľ., Klimko, T., Jankulár, M., Hovorič, R., Šottník, P., Fľaková, R., Ženišová, Z., Ondrejková, I., 2012. Arsenic and antimony contamination of waters, stream sediments and soils in the vicinity of abandoned antimony mines in the Western Carpathians, Slovakia. Appl. Geochem. 27, 598–614.

Hockmann, K., Planer-Friedrich, B., Johnston, S.G., Peiffer, S., Burton, E.D., 2020. Antimony mobility in sulfidic systems: coupling with sulfide-induced iron oxide transformations. Geochim. Cosmochim. Acta 282, 276–296.

Hu, X., He, M., Kong, L., 2015. Photopromoted oxidative dissolution of stibnite. Appl. Geochem. 61, 53–61.

Hudson-Edwards, K.A., 2019. Uptake and release of arsenic and antimony in alunite-jarosite and beudantite group minerals. Am. Mineral. 104, 633–640.

Ilgen, A.G., Trainor, T.P., 2012. Sb(III) and Sb(V) sorption onto Al-rich phases: hydrous Al oxide and the clay minerals kaolinite KGa-1b and oxidized and reduced nontronite NAu-1. Environ. Sci. Technol. 46, 843–851.

Jain, A., Loeppert, R.H., 2000. Effect of competing anions on the adsorption of arsenate and arsenite by ferrihydrite. J. Environ. Qual. 29, 1422–1430.

Johnston, S.G., Bennett, W.W., Doriean, N., Hockmann, K., Karimian, N., Burton, E.D., 2020. Antimony and arsenic speciation, redox-cycling and contrasting mobility in a mining-impacted river system. Sci. Total Environ. 710, 136354.

Johnston, S.G., Burton, E.D., Keene, A.F., Planer-Friedrich, B., Voegelin, A., Blackford, M.G., Lumpkin, G.R., 2012. Arsenic mobilization and iron transformations during sulfidization of As(V)-bearing jarosite. Chem. Geol. 334, 9–24.

Jurkovic, L., Juhásová, J., Kulikova, T., Faragó, T., Méres, S., Klimko, T., Šottník, P., Hiller, E., Nemcek, L., Bujdoš, M., 2019a. Geochemical and mineralogical exploration of soils affected by mining activities at the abandoned Sb-deposit Čučma. Miner. Slovaca 51, 217–232.

Jurkovič, Ľ., Majzlan, J., Hiller, E., Klimko, T., Voleková-Lalinská, B., Méres, Š., Göttlicher, J., Steininger, R., 2019b. Natural attenuation of antimony and arsenic in soils at the abandoned Sb-deposit Poproč, Slovakia. Environ. Earth Sci. 78, 672.

Kabata-Pendias, A., Mukherjee, A.B., 2007. Trace Elements From Soil to Human. Springer-Verlag, Berlin.

Kadokura, M., Suzuki, K., Kato, T., Grabda, M., Tokoro, C., 2019. Mechanism investigation and surface complexation modeling of arsenite sorption on ferrihydrite in adsorption/co-precipitation processes. Proceedings of the 10th European Metallurgical Conference (EMC) 2019, pp. 727–738.

Karimian, N., Johnston, S.G., Burton, E.D., 2017. Antimony and arsenic behavior during Fe(II)-induced transformation of jarosite. Environ. Sci. Technol. 51, 4259–4268.

Karimian, N., Johnston, S.G., Burton, E.D., 2018. Antimony and arsenic partitioning during Fe²⁺-induced transformation of jarosite under acidic conditions. Chemosphere 195, 515–523.

Kendall, M.R., Madden, A.S., Elwood Madden, M.E., Hu, Q., 2013. Effects of arsenic incorporation on jarosite dissolution rates and reaction products. Geochim. Cosmochim. Acta 112, 192–207.

Keon, N.E., Swartz, C.H., Brabander, D.J., Harvey, C., Hemond, H.F., 2001. Validation of an arsenic sequential extraction method for evaluating mobility in sediments. Environ. Sci. Technol. 35, 2778–2784.

Kolbe, F., Weiss, H., Morgenstern, P., Wennrich, R., Lorenz, W., Schurk, K., Stanjek, H., Daus, B., 2011. Sorption of aqueous antimony and arsenic species onto akageneite. J. Colloid Interface Sci. 357, 460–465.

Komnitsas, K., Xenidis, A., Adam, K., 1995. Oxidation of pyrite and arsenopyrite in sulphidic spoils in Lavrion. Miner. Eng. 8, 1443–1454.

Kossoff, D., Welch, M.D., Hudson-Edwards, K.A., 2015. Scorodite precipitation in the presence of antimony. Chem. Geol. 406, 1–9.

Lalinská-Voleková, B., Majzlan, J., Klimko, T., Chovanovan, M., Kucerová, G., Michnová, J., Hovoric, R., Göttlicher, J., Steininger, R., 2012. Mineralogy of weathering products of Fe-As-Sb mine wastes and soils at several Sb deposits in Slovakia. Can. Mineral. 50, 481–500.

Lee, W.C., Kim, S.-O., Ranville, J., Yun, S.-T., Choi, S.H., 2014. Sequestration of arsenate from aqueous solution using 2-line ferrihydrite: equilibria, kinetics, and X-ray absorption spectroscopic analysis. Environ. Earth Sci. 71, 3307–3318.

Leverett, P., Reynolds, J.K., Roper, A.J., Williams, P.A., 2012. Tripuhyite and schafarzikite: two of the ultimate sinks for antimony in the natural environment. Mineral. Mag. 76, 891–902.

Leuz, A.-K., Monch, H., Johnson, C.A., 2006. Sorption of Sb (III) and Sb (V) to goethite: influence on Sb (III) oxidation and mobilization. Environ. Sci. Technol. 40, 7277–7282.

Li, L., Tu, H., Zhang, S., Wu, L., Wu, M., Tang, Y., Wu, P., 2019. Geochemical behaviors of antimony in mining-affected water environment (Southwest China). Environ. Geochem. Health 41, 2397–2411.

Li, J., Zheng, B., He, Y., Zhou, Y., Chen, X., Ruan, S., Yang, Y., Dai, C., Tang, L., 2018. Antimony contamination, consequences and removal techniques: a review. Ecotoxicol. Environ. Saf. 156, 125–134.

Li, Y., Mohan, D., Pittman, C.U., Ok, Y.S., Dou, X., 2016. Removal of antimonate and antimonite from water by schwertmannite granules. Desalin. Water Treat. 57, 25639–25652.

Lin, Z., Puls, R.W., 2000. Adsorption, desorption and oxidation of arsenic affected by clay minerals and aging process. Environ. Geol. 39, 753–759.

Loni, P.C., Wu, M., Wang, W., Wang, H., Ma, L., Liu, C., Song, Y., Tuovinen, O.H., 2020. Mechanism of microbial dissolution and oxidation of antimony in stibnite under ambient conditions. J. Hazard. Mater. 385, 121561.

Majzlan, J., Lalinská, B., Chovan, M., Bläß, U., Brecht, B., Göttlicher, J., Steininger, R., Hug, K., Ziegler, S., Gescher, J., 2011. A mineralogical, geochemical, and microbiogical assessment of the antimony- and arsenic-rich neutral mine drainage tailings near Pezinok, Slovakia. Am. Mineral. 96, 1–13.

Majzlan, J., Števko, M., Lánczos, T., 2016. Soluble secondary minerals of antimony in Pezinok and Kremnica (Slovakia) and the question of mobility or immobility of antimony in mine waters. Environ. Chem. 13, 927–935.

Manaka, M., Yanase, N., Sato, T., Fukushi, K., 2007. Natural attenuation of antimony in mine drainage water. Geochem. J. 41, 17–27.

Mandal, B.K., Suzuki, K.T., 2002. Arsenic round the world: a review. Talanta 58, 201–235.

Manning, B.A., Goldberg, S., 1996. Modeling competitive adsorption of arsenate with phosphate and molybdate on oxide minerals. Soil Sci. Soc. Am. J. 60, 121–131.

McBride, M.B., 1994. Environmental Chemistry of Soils. Oxford University Press Inc, New York.

Mitsunobu, S., Takahashi, Y., Utsunomiya, S., Marcus, M.A., Terada, Y., Iwamura, T., Sakata, M., 2011. Identifcation and characterization of nanosized tripuhyite in soil near Sb mine tailings. Am. Mineral. 96, 1171–1181.

Mitsunobu, S., Takahashi, Y., Terada, Y., Sakata, M., 2010. Antimony(V) incorporation into synthetic ferrihydrite, goethite, and natural iron oxyhydroxides. Environ. Sci. Technol. 44, 3712–3718.

Moldovan, B.J., Jiang, D.T., Hendry, M.J., 2003. Mineralogical characterization of arsenic in uranium mine tailings precipitated from iron-rich hydrometallurgical solutions. Environ. Sci. Technol. 37, 873–879.

Multani, R.S., Feldmann, T., Demopoulos, G.P., 2016. Antimony in the metallurgical industry: a review of its chemistry and environmental stabilization options. Hydrometallurgy 164, 141–153.

Murciego, A.M., Sánchez, A.G., González, M.A.R., Gil, E.P., Gordillo, C.T., Fernández, J.C., Triguero, T.B., 2007. Antimony distribution and mobility in topsoils and plants (*Cytisus striatus*, *Cistus ladanifer* and *Dittrichia viscosa*) from polluted Sb-mining areas in Extremadura (Spain). Environ. Pollut. 145, 15–21.

Okkenhaug, G., Zhu, Y.-G., Luo, L., Lei, M., Li, X., Mulder, J., 2011. Distribution, speciation and availability of antimony (Sb) in soils and terrestrial plants from an active Sb mining area. Environ. Pollut. 159, 2427–2434.

Oorts, K., Smolders, E., Degryse, F., Buekers, J., Gascó, G., Cornelis, G., Mertens, J., 2008. Solubility and toxicity of antimony trioxide (Sb_2O_3) in soil. Environ. Sci. Technol. 42, 4378–4383.

Paikaray, S., Essilfie-Dughan, J., Göttlicher, J., Pollok, K., Peiffer, S., 2014. Redox stability of As(III) on schwertmannite surfaces. J. Hazard. Mater. 265, 208–216.

Paktunc, D., Dutrizac, J., Gertsman, V., 2008. Synthesis and phase transformations involving scorodite, ferric arsenate and arsenical ferrihydrite: implications for arsenic mobility. Geochim. Cosmochim. Acta 72, 2649–2672.

Pérez-López, R., Álvarez-Valero, A.M., Nieto, J.M., Sáez, R., Matos, J.X., 2008. Use of sequential extraction procedure for assessing the environmental impact at regional scale of the São Domingos Mine (Iberian Pyrite Belt). Appl. Geochem. 23, 3452–3463.

Pueyo, M., Sastre, J., Hernández, E., Vidal, M., López-Sánchez, J.F., Rauret, G., 2003. Heavy metals in the environment: prediction of trace element mobility in contaminated soils by sequential extraction. J. Environ. Qual. 32, 2054–2066.

Pueyo, M., Mateu, J., Rigol, A., Vidal, M., López-Sánchez, J.F., Rauret, G., 2008. Use of the modified BCR three-step sequential extraction procedure for the study of trace element dynamics in contaminated soils. Environ. Pollut. 152, 330–341.

Qi, C., Wu, F., Deng, Q., Liu, G., Mo, C., Liu, B., Zhu, J., 2011. Distribution and accumulation of antimony in plants in the super-large Sb deposit areas, China. Microchem. J. 97, 44–51.

Qin, X., Deng, J., Lai, H., Zhang, X., 2017. Beneficiation of antimony oxide ore: a review. Russ. J. Non-Ferr. Met. 58, 321–329.

Rakshit, S., Sarkar, D., Datta, R., 2015. Surface complexation of antimony on kaolinite. Chemosphere 119, 349–354.

Rauret, G., López-Sánchez, J.F., Sahuquillo, A., Rubio, R., Davidson, C., Ure, A., Quevauviller, P., 1999. Improvement of the BCR three step sequential extraction procedure prior to the certification of new sediment and soil reference materials. J. Environ. Monit. 1, 57–61.

Reimann, C., Matschullat, J., Birke, M., Salminen, R., 2010. Antimony in the environment: lessons from geochemical mapping. Appl. Geochem. 25, 175–198.

Ren, B., Zhou, Y., Ma, H., Deng, R., Zhang, P., Hou, B., 2018. Sb release characteristics of the solid waste produced in antimony mining smelting process. J. Mater. Cycles Waste Manag. 20, 193–200.

Ritchie, V.J., Ilgen, A.G., Mueller, S.H., Trainor, T.P., Goldfarb, R.J., 2013. Mobility and chemical fate of antimony and arsenic in historic mining environments of the Kantishna Hills district, Denali National Park and Preserve, Alaska. Chem. Geol. 335, 172–188.

Roper, A.J., Williams, P.A., Filella, M., 2012. Secondary antimony minerals: phases that control the dispersion of antimony in the supergene zone. Chem. Erde Geochem. 72 (S4), 9–14.

Saerens, A., Ghosh, M., Verdonck, J., Godderis, L., 2019. Risk of cancer for workers exposed to antimony compounds: a systematic review. Int. J. Environ. Res. Public Health 16, 4474.

Savage, K.S., Bird, D.K., O'Day, P.A., 2005. Arsenic speciation in synthetic jarosite. Chem. Geol. 215, 473–498.

Selim, H.M., 2012. Competitive Sorption and Transport of Heavy Metals in Soils and Geological Media. CRC Press, Florida.

Sobek, A.A., Schuller, W.A., Freeman, J.R., Smith, R.M., 1978. Field and Laboratory Methods Applicable to Overburden and Minesoils. US EPA, Cincinnati, Ohio (EPA 600/2-78-054).

Sun, Q., Cui, P.-X., Liu, C., Peng, S.-M., Alves, M.E., Zhou, D.-M., Shi, Z.-Q., Wang, Y.-J., 2019. Antimony oxidation and sorption behavior on birnessites with different properties (Δ-MnO_2 and triclinic birnessite). Environ. Pollut. 246, 990–998.

Sundar, S., Chakravarty, J., 2010. Antimony toxicity. Int. J. Environ. Res. Public Health 7, 4267–4277.

Thanabalasingam, P., Pickering, W.F., 1990. Specific sorption of antimony (III) by the hydrous oxides of Mn, Fe and Al. Water Air Soil Pollut. 49, 175–185.

Türk, T., Boyraz, T., Alp, İ., 2020. Arsenic removal from groundwater in Kütahya, Turkey, by novel calcined modified hydrotalcite. Environ. Geochem. Health 42, 1335–1345.

Verbeeck, M., Moens, C., Gustafsson, J.P., 2021. Mechanisms of antimony ageing in soils: an XAS study. Appl. Geochem. 128, 104936.

Vinayakumar, V., Shaji, S., Avellaneda, D., Aguilar-Martínez, J.A., Krishnan, B., 2018. Copper antimony sulfide thin films for visible to near infrared photodetector applications. RSC Adv. 8, 31055–31065.

Vink, B.W., 1996. Stability relations of antimony and arsenic compounds in the light of revised and extended Eh-pH diagrams. Chem. Geol. 130, 21–30.

Wang, S., Mulligan, C.N., 2006. Natural attenuation processes for remediation of arsenic contaminated soils and groundwater. J. Hazard. Mater. 138, 459–470.

Wang, S., Mulligan, C.N., 2008. Speciation and surface structure of inorganic arsenic in solid phases: a review. Environ. Int. 34, 867–879.

Waychunas, G.A., Rea, B.A., Fuller, C.C., Davis, J.A., 1993. Surface chemistry of ferrihydrite: part 1. EXAFS studies of the geometry of coprecipitated and adsorbed arsenate. Geochim. Cosmochim. Acta 57, 2251–2269.

Wedepohl, K.H., 1995. The composition of the continental crust. Geochim. Cosmochim. Acta 59, 1217–1232.

Wenzel, W.W., Kirchbaumer, N., Prohaska, T., Stingeder, G., Lombi, E., Adriano, D.C., 2001. Arsenic fractionation in soils using an improved sequential extraction procedure. Anal. Chim. Acta 436, 309–323.

Wilson, S.C., Lockwood, P.V., Ashley, P.M., Tighe, M., 2010. The chemistry and behaviour of antimony in the soil environment with comparisons to arsenic: a critical review. Environ. Pollut. 158, 1169–1181.

Wu, F., Fu, Z., Liu, B., Mo, C., Chen, B., Corns, W., Liao, H., 2011. Health risk associated with dietary co-exposure to high levels of antimony and arsenic in the world's largest antimony mine area. Sci. Total Environ. 409, 3344–3351.

Xi, J., He, M., Kong, L., 2016. Adsorption of antimony on kaolinite as a function of time, pH, HA and competitive anions. Environ. Earth Sci. 75, 1–7.

Xi, J., He, M., Lin, C., 2010. Adsorption of antimony(V) on kaolinite as a function of pH, ionic strength and humic acid. Environ. Earth Sci. 60, 715–722.

Xi, J., He, M., Zhang, G., 2014. Antimony adsorption on kaolinite in the presence of competitive anions. Environ. Earth Sci. 71, 2989–2997.

Yan, L., Chan, T., Jing, C., 2020. Mechanistic study for stibnite oxidative dissolution and sequestration on pyrite. Environ. Pollut. 262, 114309.

Yeh, N.-T., Chiu, P.-C., Chyi, J.-I., Ren, F., Pearton, S.J., 2013. Sb-based semiconductors for low power electronics. J. Mater. Chem. C 1, 4616–4627.

Zhang, X., Friedrich, S., Liu, B., Huang, T., Friedrich, B., 2020. Computation-assisted analyzing and forecasting on impurities removal behavior during zone refining of antimony. J. Mater. Res. Technol. 9, 1221–1230.

Zhang, Y., Ren, B., Hursthouse, A., Deng, R., Hou, B., 2019. Leaching and releasing characteristics and regularities of Sb and As from antimony mining waste rocks. Pol. J. Environ. Stud. 28, 4017–4025.

Zhang, Z., Bi, X., Li, X., Zhao, Q., Chen, H., 2018. Schwertmannite: occurrence, properties, synthesis and application in environmental remediation. RSC Adv. 8, 33583–33599.

Zhou, S., Deng, R., Hursthouse, A., 2020. Risk assessment of potentially toxic elements pollution from mineral processing steps at xikuangshan antimony plant, Hunan,China. Processes 8, 29.

Zhou, S., Hursthouse, A., 2019. The impact of physical properties on the leaching of potentially toxic elements from antimony ore processing wastes. Int. J. Environ. Res. Public Health 16, 2355.